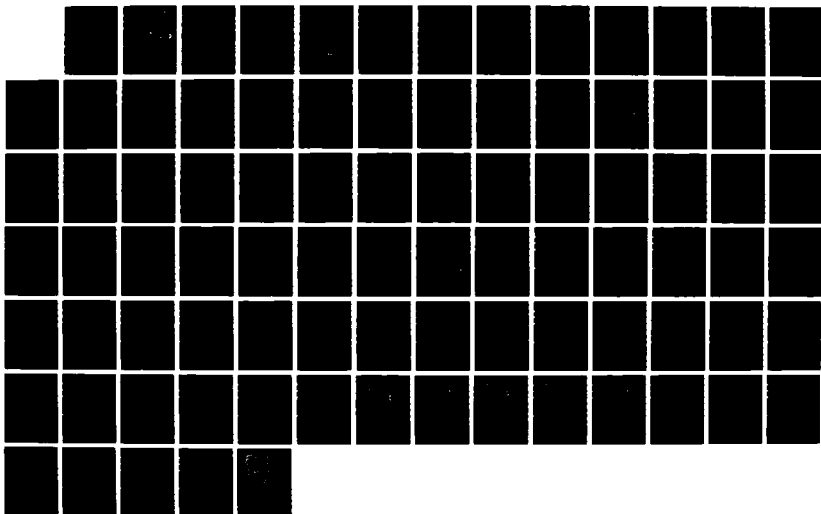


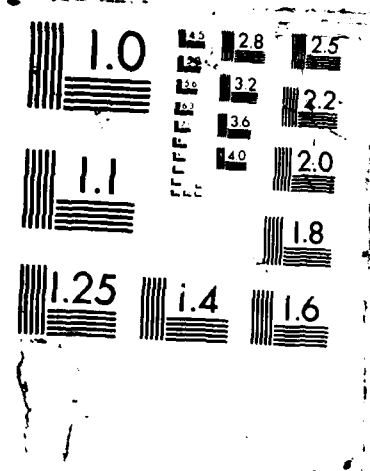
AD-A190 013

A COMPUTERIZED INVESTIGATION USING THE METHOD OF IMAGES 1/1  
TO PREDICT THE SO. (U) NAVAL POSTGRADUATE SCHOOL  
MONTEREY CA C KASHANDI DEC 87

UNCLASSIFIED

F/G 20/1 NL





AD-A190 013

2

DTIC FILE COPY

# NAVAL POSTGRADUATE SCHOOL

Monterey, California



DTIC  
ELECTE  
MAR 18 1988  
S D  
caH

## THESIS

A Computerized Investigation Using the Method  
of Images to Predict the Sound Field in a  
Fluid Wedge Overlying a Slow Fluid Half-Space

by

Carolus Kaswandi

December 1987

Thesis Advisor:  
Thesis Advisor:

A. B. Coppens  
J. V. Sanders

Approved for public release; distribution is unlimited.

88 3 16 033

A190013

## REPORT DOCUMENTATION PAGE

1a REPORT SECURITY CLASSIFICATION <b>UNCLASSIFIED</b>		1b RESTRICTIVE MARKINGS	
2a SECURITY CLASSIFICATION AUTHORITY		3 DISTRIBUTION/AVAILABILITY OF REPORT Approved for public release; distribution is unlimited.	
2b DECLASSIFICATION/DOWNGRADING SCHEDULE		5 MONITORING ORGANIZATION REPORT NUMBER(S)	
4 PERFORMING ORGANIZATION REPORT NUMBER(S)		7a NAME OF MONITORING ORGANIZATION Naval Postgraduate School	
6a NAME OF PERFORMING ORGANIZATION Naval Postgraduate School	6b OFFICE SYMBOL (If applicable) 61	7b ADDRESS (City, State, and ZIP Code) Monterey, CA 93943-5000	
8a NAME OF FUNDING SPONSORING ORGANIZATION		9. PROCUREMENT INSTRUMENT IDENTIFICATION NUMBER	
8b OFFICE SYMBOL (If applicable)		10. SOURCE OF FUNDING NUMBERS	
8c ADDRESS (City, State, and ZIP Code)		PROGRAM ELEMENT NO.	PROJECT NO.
		TASK NO.	WORK UNIT ACCESSION NO.
11 TITLE (Include Security Classification) A COMPUTERIZED INVESTIGATION USING THE METHOD OF IMAGES TO PREDICT THE SOUND FIELD IN A FLUID WEDGE OVERLYING A SLOW FLUID HALF-SPACE. UNCLASSIFIED			
12 PERSONAL AUTHOR(S) KASWANDT, CAROLUS			
13a TYPE OF REPORT MASTER'S THESIS	13b TIME COVERED FROM TO	14. DATE OF REPORT (Year, Month, Day) 1987 - DECEMBER	15 PAGE COUNT 86
16 SUPPLEMENTARY NOTATION			
17 COSATI CODES		18 SUBJECT TERMS (Continue on reverse if necessary and identify by block number)	
FIELD	GROUP	SUB-GROUP	
19 ABSTRACT (Continue on reverse if necessary and identify by block number) Sound fields in wedge-shaped ocean layers, modeling conditions on the continental shelf, have been studied at the Naval Postgraduate School in the last few years using the method of images. These studies are carried further in the present work. This method is implemented in different environmental conditions. This thesis examines the influence of several parameters on the sound field for downslope propagation in a wedge-shaped fluid of speed of sound $c_2$ overlying a slow bottom of speed of sound $c_1$ . On the basis of qualitative and semi-quantitative analysis of the behavior of the pressure-depth profile for various geometrical and physical parameters, we can conclude that:  1. A defined distance, the "characteristic distance" $X_0 = \pi / (2k_2 \sin \theta_0 \tan \beta)$ , where $\cos \theta_0 = c_1 / c_2$ , $k_2 = \omega / c_2$ , and $\beta$ is the vertex angle of the wedge, has physical meaning as a useful scaling distance.			
20 DISTRIBUTION AVAILABILITY OF ABSTRACT <input checked="" type="checkbox"/> UNCLASSIFIED UNLIMITED <input type="checkbox"/> SAME AS RPT <input type="checkbox"/> DTIC USERS		21 ABSTRACT SECURITY CLASSIFICATION UNCLASSIFIED	
22a NAME OF RESPONSIBLE INDIVIDUAL A. B. COPPENS		22b TELEPHONE (Include Area Code) 646-2941	22c OFFICE SYMBOL 61

UNCLASSIFIED

SECURITY CLASSIFICATION OF THIS PAGE (When Data Entered)

2. The distance of the source from the apex, in terms of the  $X_0$ , plays a major role in determining the downslope sound field.



Accession For	
NTIS GRA&I	<input checked="checked" type="checkbox"/>
DTIC TAB	<input type="checkbox"/>
Unannounced	<input type="checkbox"/>
Justification	
By	
Distribution/	
Availability Codes	
Avail and/or	
Spec	
A-1	

S N 0102- LF-014-6601

UNCLASSIFIED

SECURITY CLASSIFICATION OF THIS PAGE(When Data Entered)

Approved for public release, distribution is unlimited.

A Computerized Investigation Using the Method  
of Images to Predict the Sound Field in a  
Fluid Wedge Overlying a Slow Fluid Half-Space

by

Carolus Kaswandi  
Commander, Indonesian Navy  
B.S., Indonesian Navy Electronics School, 1967  
Eng., Indonesian Navy Institute of Science, 1979

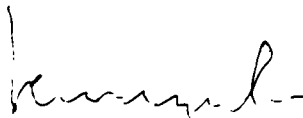
Submitted in partial fulfillment of the  
requirements for the degree of

MASTER OF SCIENCE IN PHYSICS

from the

NAVAL POSTGRADUATE SCHOOL  
December 1987

Author:



Carolus Kaswandi

Approved by:



A. B. Coppens, Thesis Advisor



J. V. Sanders, Thesis Advisor



K. Woehler, Chairman  
Department of Physics



G. E. Schacher  
Dean of Science and Engineering

# ABSTRACT

Sound fields in wedge-shaped ocean layers, modeling conditions on the continental shelf, have been studied at the Naval Postgraduate School in the last few years using the method of images. These studies are carried further in the present work. The method is implemented in different environmental conditions. This thesis examines the influence of several parameters on the sound field for downslope propagation in a wedge-shaped fluid of speed of sound  $c_2$  overlying a slow bottom of speed of sound  $c_1$ . On the basis of qualitative and semi-quantitative analysis of the behavior of the pressure-depth profile for various geometrical and physical parameters, we can conclude that:

1. A defined distance, the "characteristic distance"  $x_0 = \pi / (2k_2 \sin \theta_0 \tan \beta)$ , where  $\cos \theta_0 = c_1 / c_2$ ,  $k_2 = \omega / c_2$ , and  $\beta$  is the vertex angle of the wedge, has physical meaning as a useful scaling distance.
2. The distance of the source from the apex, in terms of the  $x_0$ , plays a major role in determining the downslope sound field.

## TABLE OF CONTENTS

I.	INTRODUCTION .....	11
A.	SOUND PROPAGATION IN THE WEDGE .....	11
B.	THE METHOD OF IMAGES .....	13
C.	A COMPUTER PROGRAM DSLOW .....	14
II.	THEORY .....	18
A.	GENERAL VIEW OF PRESSURE DISTRIBUTION IN THE WEDGE DOWNSLOPE .....	19
B.	SOUND PRESSURE AT A POINT IN THE WEDGE DOWNSLOPE PREDICTED BY THE METHOD OF IMAGES ...	28
III.	DSLOW PROGRAM IMPLEMENTATION .....	28
A.	PROGRAM FEATURES .....	28
B.	NORMALIZATION .....	29
C.	PROCEDURE .....	31
D.	PROGRAM IMPROVEMENT .....	31
IV.	DISCUSSIONS .....	45
A.	GRAPHS OUTPUT .....	45
B.	GRAPHS CLASSIFICATION .....	46
1.	Type 1 Curves .....	46
2.	Type 2 Curves .....	46
3.	Type 3 Curves .....	48
C.	TRANSITION POINT .....	48



D.	PARAMETER VARIATIONS .....	53
1.	Variations of $\beta$ .....	53
2.	Variations of $\gamma$ .....	53
3.	Variations of $c_1/c_2$ and $\rho_1/\rho_2$ .....	54
V.	CONCLUSIONS AND RECOMMENDATIONS .....	55
A.	CONCLUSIONS .....	55
B.	RECOMMENDATIONS .....	56
APPENDIX A:	DSLOW ALGORITHM .....	57
APPENDIX B:	DSLOW PROGRAM .....	60
APPENDIX C:	NUMERICAL RESULTS OF DSLOW .....	65
APPENDIX D:	TABLES .....	71
APPENDIX E:	GRAPHS OF $R_1$ VERSUS $R_2$ AT THE FIRST TRANSITION POINT .....	74
LIST OF REFERENCES	.....	82
INITIAL DISTRIBUTION LIST	.....	84

## LIST OF TABLES

1. Receiver Distance at the First Transition Point,  
for Constant  $\rho_1/\rho_2 = 0.80$ ,  $c_1/c_2 = 1.10$  ..... 71
2. Received Distance at the First Transition Point,  
for Constant  $\rho_1/\rho_2 = 0.80$ ,  $c_1/c_2 = 1.20$  ..... 72
3. Receiver Distance at the First Transition Point,  
for Constant  $\rho_1/\rho_2 = 0.90$ ,  $c_1/c_2 = 1.10$  ..... 73

# LIST OF FIGURES

1.1	Geometry of the wedge .....	17
2.1	Ray tracing in the wedge downslope .....	20
2.2	Geometry of a wedge by the method of images .....	22
2.3	Geometric development of reflection angles .....	24
2.4	Geometry of symmetric images .....	26
3.1	Pressure amplitude normalization .....	30
3.2	Graphs of receiver angle $\delta$ versus pressure amplitude with $R_2$ fixed, $R_1$ varied .....	33
3.3	Graphs of receiver angle $\delta$ versus pressure amplitude with $R_2$ fixed, $R_1$ varied .....	34
3.4	Graphs of receiver angle $\delta$ versus pressure amplitude with $R_2$ fixed, $R_1$ varied .....	35
3.5	Graphs of receiver angle $\delta$ versus pressure amplitude with $R_2$ fixed, $R_1$ varied .....	36
3.6	Graphs of receiver angle $\delta$ versus pressure amplitude with $R_2$ fixed, $R_1$ varied .....	37
3.7	Graphs of receiver angle $\delta$ versus pressure amplitude with $R_2$ fixed, $R_1$ varied .....	38
3.8	Graphs of receiver angle $\delta$ versus pressure amplitude with $R_2$ fixed, $P_1$ varied .....	39
3.9	Graphs of receiver angle $\delta$ versus pressure amplitude with $R_2$ fixed, $R_1$ varied .....	40
3.10	Graphs of receiver angle $\delta$ versus pressure amplitude with $R_2$ fixed, $R_1$ varied .....	41
3.11	Graphs of receiver angle $\delta$ versus pressure amplitude with $R_2$ fixed, $R_1$ varied .....	42
3.12	Graphs of receiver angle $\delta$ versus pressure amplitude with $R_2$ fixed, $R_1$ varied .....	43

3.13	Graphs of receiver angle $\delta$ versus pressure amplitude with $R_2$ fixed, $R_1$ varied .....	44
4.1	The plots where there are two transition points, $R_2 = 4.6$ is the first and $R_2 = 6.4$ is the second .....	47
4.2	Type 1 curves, indicating a pressure amplitude nearly linear with depth .....	50
4.3	Type 2 curves, indicating a well-collimated sound field as the source away from the apex .....	51
4.4	Type 3 curves, indicating the presence of reflection and diffraction near the bottom .....	52
E.1	$R_1$ vs $P_2$ at the first trans. points, for $\beta = 6^\circ$ , $\rho_1/\rho_2 = 0.80$ , $c_1/c_2 = 1.10$ .....	74
E.2	$R_1$ vs $P_2$ at the first trans. points, for $\beta = 10^\circ$ , $\rho_1/\rho_2 = 0.80$ , $c_1/c_2 = 1.10$ .....	75
E.3	$P_1$ vs $R_2$ at the first trans. points, for $\beta = 15^\circ$ , $\rho_1/\rho_2 = 0.80$ , $c_1/c_2 = 1.10$ .....	76
E.4	$P_1$ vs $R_2$ at the first trans. points, for $\beta = 6^\circ$ , $\rho_1/\rho_2 = 0.80$ , $c_1/c_2 = 1.20$ .....	77
E.5	$P_1$ vs $P_2$ at the first trans. points, for $\beta = 10^\circ$ , $\rho_1/\rho_2 = 0.80$ , $c_1/c_2 = 1.10$ .....	78
E.6	$R_1$ vs $R_2$ at the first trans. points, for $\beta = 15^\circ$ , $\rho_1/\rho_2 = 0.80$ , $c_1/c_2 = 1.10$ .....	79
E.7	$P_1$ vs $P_2$ at the first trans. points, for $\beta = 6^\circ$ , $\rho_1/\rho_2 = 0.90$ , $c_1/c_2 = 1.10$ .....	80
E.3	$R_1$ vs $P_2$ at the first trans. points, for $\beta = 10^\circ$ , $\rho_1/\rho_2 = 0.90$ , $c_1/c_2 = 1.10$ .....	81

## ACKNOWLEDGEMENTS

I would like to acknowledge Professor Alan B. Coppens who assigned this interesting topic. My thanks to Commander Chil Ki Baek who assisted Professor Alan B. Coppens thus making this job much easier. I thank my wife Tuti and my children, Henry, Anna, and Michael, for their patience and support. I thank those people in the Physics Department of the Naval Postgraduate School who encouraged me to persevere.

Finally, I hope that in the future this work will be useful to others by expanding their knowledge in this field.

## I. INTRODUCTION

### A. SOUND PROPAGATION IN SHALLOW WATER CHANNEL

Experimental investigations of sound propagation in shallow water channels have been done by several investigators. Shallow water propagation is of interest because of the applications to coastal defense. These investigations are expensive and time consuming. The use of a computer model should provide a relatively inexpensive alternative to observation.

One of the techniques uses normal mode theory. The normal mode theory, which was introduced and developed by C. L. Pekeris [Ref. 1], gave the exact solution in water of constant depth. Further development of normal mode theory was made by L. Brekovskikh [Ref. 2], who initiated pressure as an integral involving Bessel functions and solution of the normal mode equation. Another theoretical approach to sound propagation in a horizontally stratified ocean of constant depth is given by the method of multiple scattering [Ref. 1]. With this method, all the previous theories can be simplified by conversion into an asymptotic form which is valid when the acoustic wavelength is small compared to the distance over which the sound speed varies appreciably. These theories agree with the laboratory experiments.

For a water channel with a small bottom slope, the sound field may be expressed approximately in terms of adiabatic normal modes. To facilitate prediction, R.D. Groves, Anton Nagl, H. Uberall, and G. L. Zauer [Ref. 3] modeled a wedge-shaped isovelocity ocean with a linearly-sloping, perfectly-rigid ocean floor using adiabatic normal modes. For a penetrable bottom the normal mode description fails when modes propagating upslope encounter the "critical depth" ( $H_c$ ), defined as the depth where the associate mode changes from fully trapped within the water channel to radiating energy into the bottom (cut off) [Ref. 4-6]. The parabolic equation can be used to explain the mechanism of sound energy radiation into the bottom [Ref. 7,8]. Such an equation was studied by F. B. Jensen and W. A. Kuperman [Ref. 9], with predictions that satisfactorily agreed with the experimental results for small ray angles. With some restrictions, normal mode theory is applicable for sound propagation in the wedge-shaped fluid with a fast bottom. The parabolic equation is good for fast and slow bottom, but with the restriction that horizontal ray angles must be less than  $20^\circ$ .

Another technique introduced to predict the propagation of sound in the wedge is the method of images. This method was derived from the simplest case; a monofrequency point source in a homogeneous ocean with parallel boundaries. The total pressure is the sum of an infinite number of spherical

waves from an infinite set of images. The restriction of this method is that it does not generalize to the case of inhomogeneous media or non-planar boundaries. In this work, this method will be studied.

### 3. THE METHOD OF IMAGES

In 1978, Connors, Sanders, Ioannou, and Kawamura [Ref. 10], predicted the pressure amplitude and phase of the sound field along the bottom of a wedge-shaped fluid layer of density  $\rho_1$ , and speed of sound  $c_1$ , overlying a fast fluid bottom of density  $\rho_2$ , and speed of sound  $c_2 > c_1$  by applying the method of images in a computer program implementation. In 1984, Baek [Ref. 11], and LeSesne [Ref. 12], implemented further improvements. Baek's computer program, WEDGE, and LeSesne's computer program XSLOPE were validated for several cases. WEDGE was developed for two-dimensional upslope propagation (the source and receiver are in the same vertical plane perpendicular to the shore line, and the receiver is closer to the apex than the source (Figure 1.1a)) and downslope propagation (the source is closer to the apex than the receiver (Figure 1.1b)). XSLOPE was developed for upslope, downslope, or cross-slope propagation (the source, receiver, and apex, are not necessarily in the same plane perpendicular to the shore line (Figure 1.1c)). In both programs, Baek and LeSesne assume that the fluid in the wedge and fluid in the bottom have constant densities, that



the speed of sound is constant, and that the interface between the fluids and the surface is smooth.

In both WEDGE and XSLOPE, all distances are scaled in units of the "dump distance." A dump distance  $X$ , as stated in Reference 10, is the distance from the apex measured along the interface at which the lowest mode attains cutoff. If the wedge angle is  $\beta$  (Figure 1.1c), then

$$X = \frac{\pi/2}{k_1 \sin \theta_c \tan \beta} \quad (1.1)$$

$$\theta_c = \arccos(c_1/c_2) \quad (1.2)$$

where  $k_1$  is the wave number in the wedge and  $\theta_c$  is the critical grazing angle for reflection of sound from the bottom. For  $\beta \ll 1$

$$X = H \tan \beta \quad (1.3)$$

This scaling distance negates the necessity of specifying frequency.

#### C. COMPUTER PROGRAM DSLOW

At the start of the work reported in this thesis, a computer program was obtained [Ref. 13], which is an extension of the WEDGE and XSLOPE for downslope configuration with a slow bottom. The computer model, DSLOW, developed to run on a desktop computer (Wang 2000), uses the method of images to predict the pressure amplitude and phase anywhere

within the wedge fluid overlying a slow bottom in a cross-slope configuration. A geometrical picture of this configuration is shown in Figure 1.1c.

Mathematically, the model used in WEDGE and XSLOPE is applicable in any condition. But consideration must be given for making it work for a slow bottom. In the case of a fast bottom, the dump distance has a physical meaning. The dump distance is expressed as a function of the critical angle. The critical angle is equal to  $\arccos(c_1/c_2)$ . In the case of slow bottom,  $c_1/c_2$  is greater than 1, thus  $\arccos(c_1/c_2)$  is invalid; therefore, so is the dump distance. To facilitate the scaling factor, a "characteristic distance" or "scaling distance" is introduced. We need the scaling distance because, with this distance, our model will be independent of frequency as in the fast bottom case. There is also the hope that the use of a scaling distance will allow systematic observation of the pressure field. This scale distance  $X_0$  is the distance measured along the interface from the apex to the point where the lowest mode would attain cutoff if the fluids in the wedge and in the bottom were to be interchanged. The characteristic distance is defined by the following equation:

$$X_0 = \frac{\pi/2}{\kappa_2 \sin\theta_0 \tan\beta} \quad (1.4)$$

where  $\theta_0 = \arccos(c_2/c_1)$  and  $K_2 = \omega/c_2$  is the wave number in the bottom.

The following terms will be used throughout (see Figure 1.1):

$\beta$  = wedge angle

$R_1$  = distance of the source from the apex in units of  $X_0$

$R_2$  = distance of the receiver from the apex in units of  $X_0$

$\gamma$  = angle of elevation of the source above the bottom

$\delta$  = angle of elevation of the receiver above the bottom

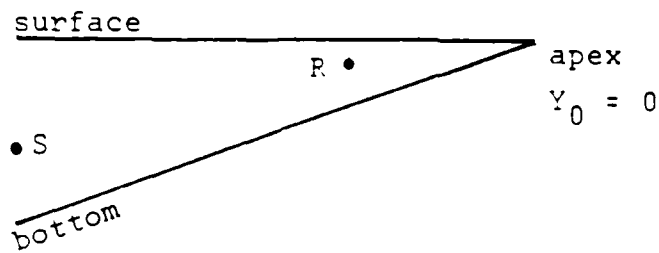
$Y_0$  = distance between the projection of the source and receiver on the shore line, scaled by  $X_0$

$\rho_1/\rho_2$  is the ratio between the density of the fluid in the wedge ( $\rho_1$ ) and the density of the fluid in the bottom ( $\rho_2$ )

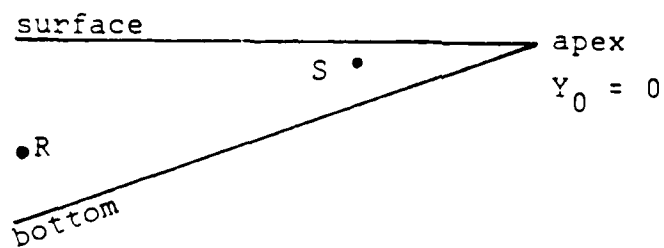
$c_1/c_2$  is the ratio between the speed of sound in the wedge ( $c_1$ ) and the speed of sound in the bottom ( $c_2$ ). A fast bottom occurs when  $c_2 > c_1$ ; a slow bottom occurs when  $c_2 < c_1$

The purpose of this research is the following:

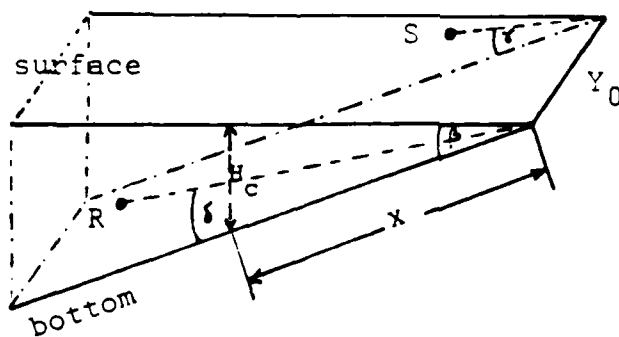
1. To transfer, test, and evaluate DSLOW program on the IBM 3300;
2. To obtain numerical and graphical output for a number of cases; and
3. To attempt to develop plausible explanations for any significant features observed.



a. upslope configuration



b. downslope configuration



c. cross-slope configuration

Figure 1.1 Geometry of the wedge

## II. THEORY

### A. GENERAL VIEW OF A WEDGE PRESSURE DISTRIBUTION IN THE DOWNSLOPE CONFIGURATION

A general picture of the sound energy propagation within the wedge in downslope direction is given in Figure 2.1. If a sound source is placed at point S, ray 1 will reach the surface at point P with an incident angle  $\alpha$  with respect to the normal to the surface at this point. This ray is reflected by the surface at the same angle but with the phase  $180^\circ$  different. (On the surface, sound pressure is zero everywhere.) The reflected ray reaches the bottom with an incident angle  $\beta + \alpha$ . At great enough distance, ray 1 never reaches the bottom again. This ray does not contribute to a sound pressure field at the bottom. The pressure at the bottom should be very small according to the ray theory argument.

Using these ray-tracing methods, an estimated profile of the pressure amplitude versus the receiver depth can be made. When the source and the receiver are placed near the apex, the pressure amplitude is zero at the surface, a maximum somewhere within the wedge, and greater than zero at the bottom. In the case where the source is at a far distance, the pressure amplitude is equal to zero at the surface, a maximum somewhere within the wedge, and zero at the bottom.

Ray tracing will only give a rough approximation, not an exact solution, but ray tracing may be used as a guide. The method of images calculates the exact pressure amplitude at each point within the wedge subject only to the assumption inherent in using the plane-wave Rayleigh reflection coefficients.

#### B. SOUND PRESSURE AT A POINT IN THE WEDGE DOWNSLOPE PREDICTED BY THE METHOD OF IMAGES

Let the source be a scaled distance  $R_1$  from the apex and at an angle of  $\gamma$  measured from the bottom of the wedge. Let the receiver be a scaled distance  $R_2$  from the apex and at an angle  $\delta$  measured from the bottom.

Using Figure 2.2, let the upper half family of images be  $n = 1, 2, 3, 4, \dots$  and the lower half family be  $n' = 1, 2, 3, 4, \dots$ . Calculating the field resulting from source and images proceeds along the lines developed in [Ref. 14]. If  $\phi_n$  is the angle formed at the apex between the  $n_{th}$  image of the source and the receiver, then

$$\phi_1 = 2\beta - \delta - \gamma$$

$$\phi_2 = 2\beta - \delta + \gamma$$

$$\phi_3 = 4\beta - \delta - \gamma$$

$$\phi_4 = 4\beta - \delta + \gamma$$

....

....

....

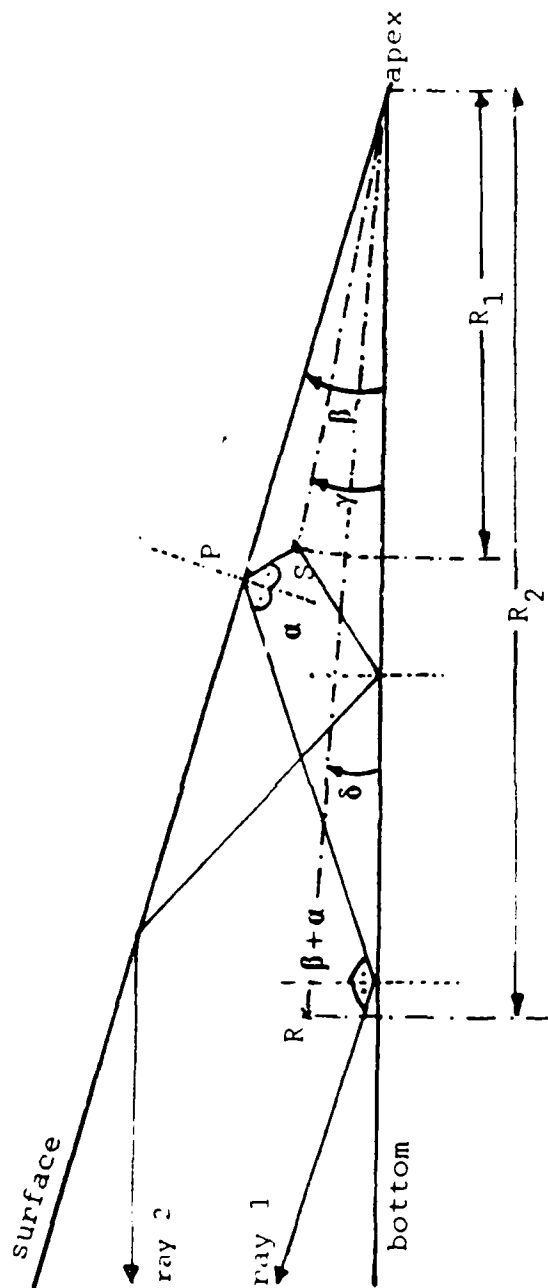


Figure 2.1 Ray tracing in the wedge downslope

or more generally

$$\phi_n = (n + 1)\beta - \delta - \gamma \quad \text{for } n \text{ odd}$$

$$\phi_n = n\beta - \delta + \gamma \quad \text{for } n \text{ even}$$

Which can be reduced to:

$$\phi_n = \{n + (1/2)[1 - (-1)^n]\}\beta + (-1)^n\gamma - \delta \quad (2.1)$$

or

$$\phi_n = 2 \text{ INT} \left[ \frac{n + 1}{2} \right] \beta + (-1)^n\gamma - \delta \quad (2.2)$$

where  $\text{INT}[ ]$  denotes the largest integer which is equal to, or smaller than the argument. Using the same method for the member  $n'$  of the lower family of images we obtain:

$$\phi_{n'} = \{n + (1/2)[1 - (-1)^n]\}\beta + (-1)^n\gamma + \delta \quad (2.3)$$

or

$$\phi_{n'} = 2 \text{ INT} \left[ \frac{n + 1}{2} \right] \beta + (-1)^n\gamma + \delta \quad (2.4)$$

Using the geometry of Figures 2.2 and 2.4, the distance between the  $n^{\text{th}}$  and  $n'^{\text{th}}$  images to the receiver is respectively

$$r_n = \sqrt{R_1^2 + R_2^2 - 2R_1R_2\cos\phi_n} \quad (2.5)$$

and

$$r_{n'} = \sqrt{R_1^2 + R_2^2 - 2R_1R_2\cos\phi_{n'}} \quad (2.6)$$



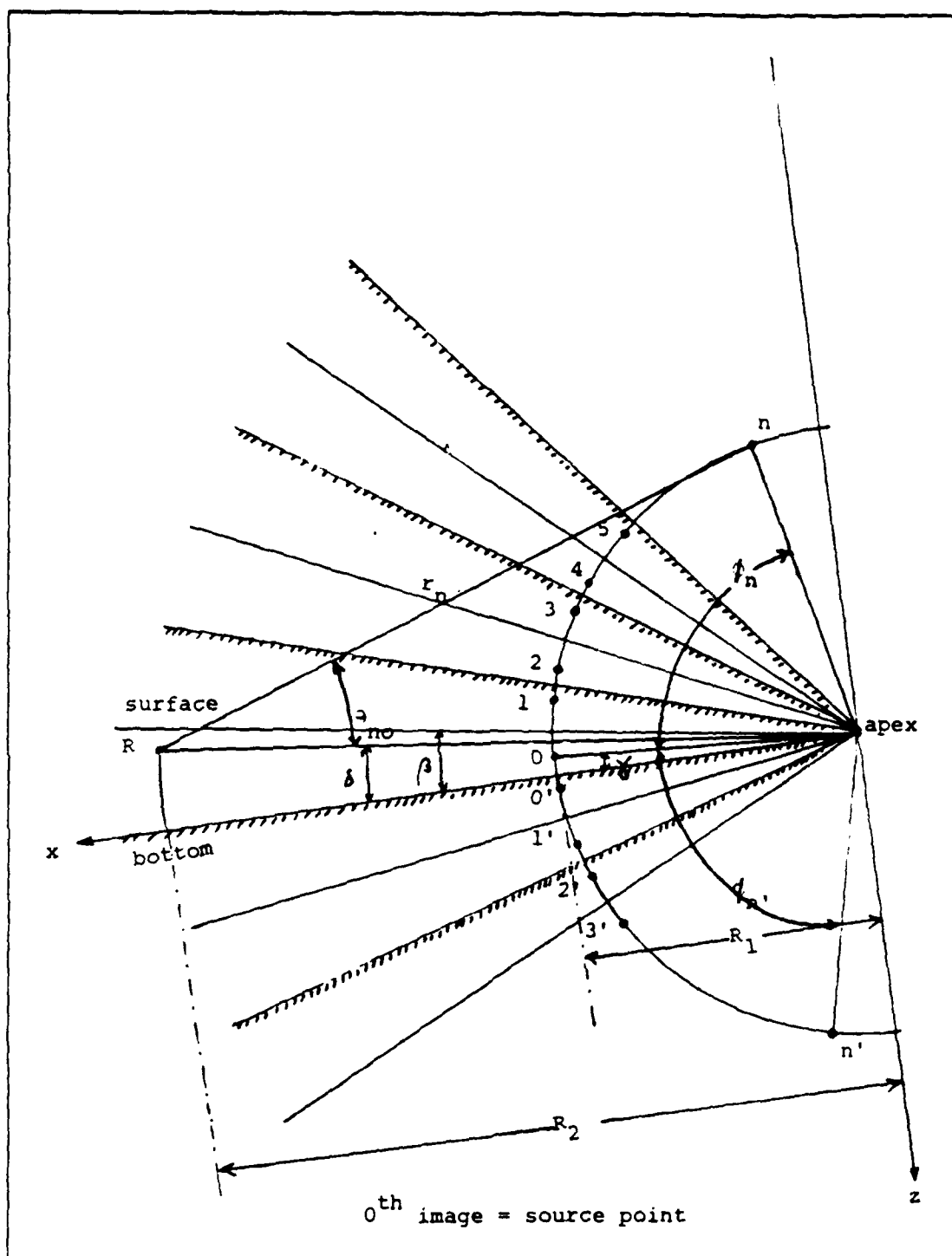


Figure 2.2 Geometry of a wedge by the method of images

The angles  $\theta_{no}$  and  $\theta_{n'o}$  for the  $n^{\text{th}}$  and  $n'^{\text{th}}$  images respectively are

$$\theta_{no} = \arctan \left[ \frac{\sin \phi_n}{R_2/P_1 - \cos \phi_n} \right] \quad (2.7)$$

and

$$\theta_{n'o} = \arctan \left[ \frac{\sin \phi_{n'}}{R_2/P_1 - \cos \phi_{n'}} \right] \quad (2.8)$$

Define  $\theta_{nm}$  and  $\theta_{n'm}$  as the angles of incidence for the  $m^{\text{th}}$  bounces from the bottom for the  $n$  and  $n'$  image respectively;  $m = 1, 2, 3, \dots$  (The  $0^{\text{th}}$  bounce is the last one before reaching the receiver.) The geometry of Figures 2.2 and 2.3 give  $\theta_{nm}$  as follows:

$$\theta_{21} = \theta_{20} - 2\beta - \delta$$

$$\theta_{32} = \theta_{30} - 4\beta - \delta$$

$$\theta_{41} = \theta_{40} - 2\beta - \delta$$

$$\theta_{52} = \theta_{50} - 4\beta - \delta$$

....

....

....

The general expression is

$$\theta_{nm} = \theta_{no} - 2m\beta - \delta$$

Using the same method

$$\theta_{n'm} = \theta_{n'o} - 2m\beta + \delta$$

The maximum number of bottom bounces of the  $n^{\text{th}}$  and  $n'^{\text{th}}$  image is

$$m_{\max} = M = \text{INT} [\phi_n/2\beta] = \text{INT} [\phi_{n'}/2\beta]$$

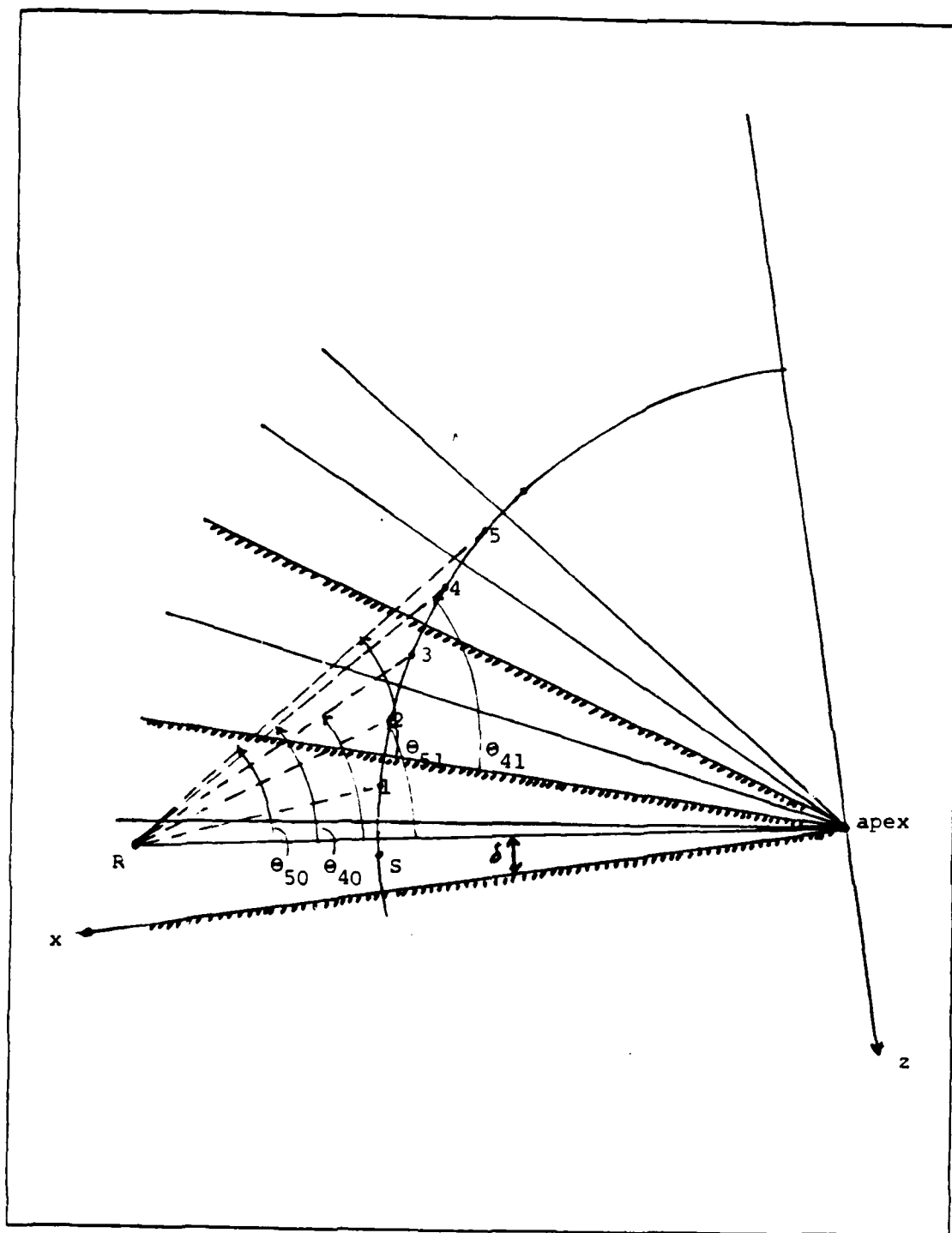


Figure 2.3 Geometric development of reflection angles

The maximum number of images is

$$n_{\max} = N = \text{INT} [\pi/\beta]$$

The reflection coefficients for the  $n^{\text{th}}$  and  $n'^{\text{th}}$  images for a plane wave are:

$$R(\theta_{nm}) = \frac{\frac{\rho_1 c_1}{\rho_2 c_2} - \psi_{nm}}{\frac{\rho_1 c_1}{\rho_2 c_2} + \psi_{nm}} \quad (2.9)$$

and

$$R(\theta_{n'm}) = \frac{\frac{\rho_1 c_1}{\rho_2 c_2} - \psi_{n'm}}{\frac{\rho_1 c_1}{\rho_2 c_2} + \psi_{n'm}} \quad (2.10)$$

where

$$\psi_{nm} = \frac{\sqrt{1 - (c_1/c_2)^2 \cos^2 \theta_{nm}}}{\sin \theta_{nm}} \quad (2.11)$$

and

$$\psi_{n'm} = \frac{\sqrt{1 - (c_1/c_2)^2 \cos^2 \theta_{n'm}}}{\sin \theta_{n'm}} \quad (2.12)$$

The contribution from the upper family of images is

$$P_u = \sum_{n=1}^N \frac{1}{r_n} \exp(-jkr_n) (-1)^{\text{INT}[n+1)/2]} \prod_{m=0}^M R_{nm} \quad (2.13)$$

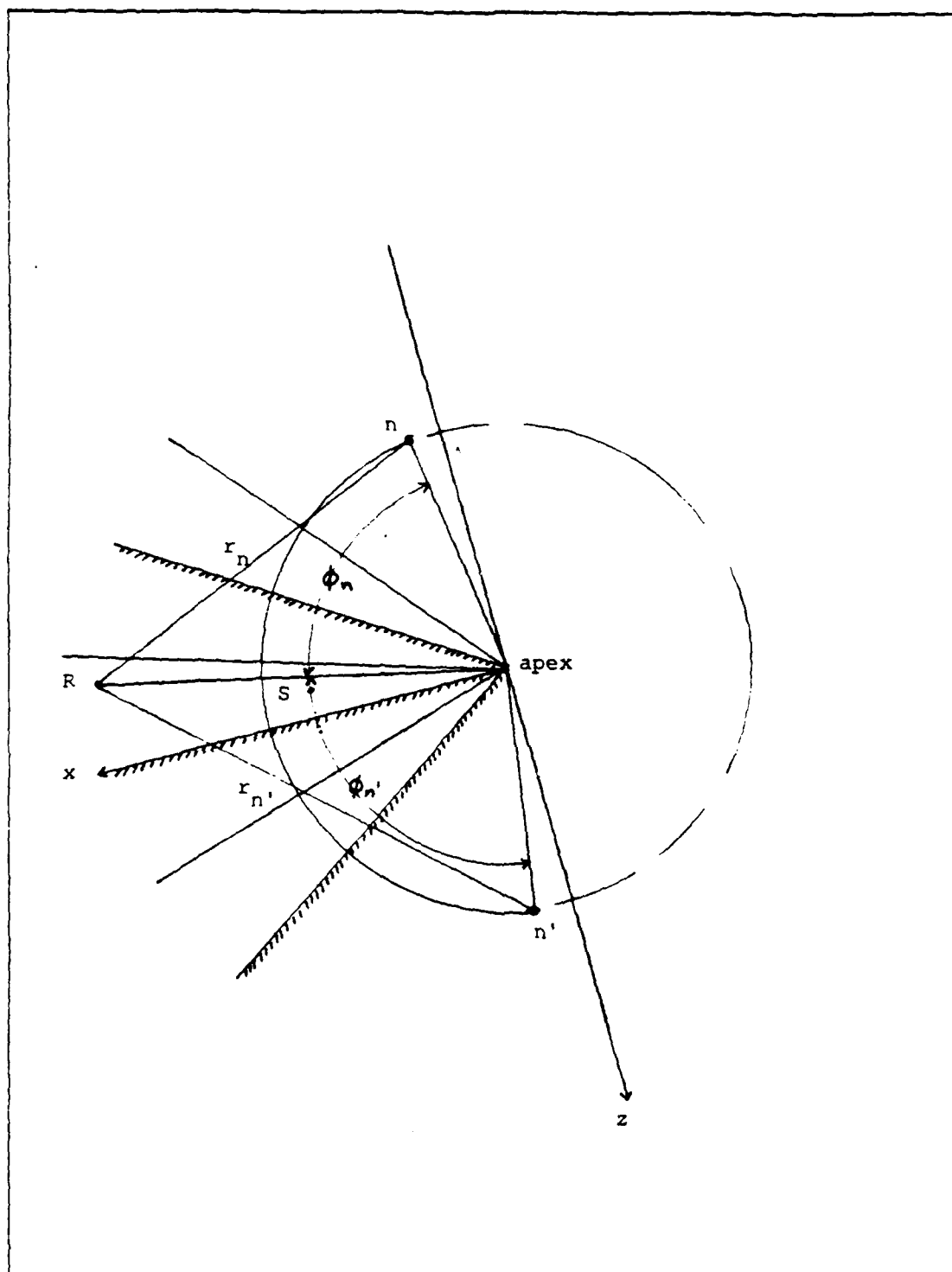


Figure 2.4 Geometry of symmetric images

and for lower family of images is

$$P_u = \sum_{n=1}^N \frac{1}{r_n} \exp(-jkr_n) (-1)^{\text{INT}[n+1)/2]} \prod_{m=0}^M R_n^m \quad (2.14)$$

The total complex pressure is

$$P(x) = P_u + P_l \quad (2.15)$$

### III. DSLOW PROGRAM IMPLEMENTATION

#### A. PROGRAMS FEATURES

Since the mainframe graphics computer was available, the DISSPLA graphical program was used. The only programming language compatible with DISSPLA is FORTRAN. The numerical and graphical output is provided by this program. To give the pressure amplitude versus received angle graphs, two-dimensional plotting is used.

The program DSLOW is run by placing the point source anywhere in the wedge and then placing the receiver at a distance downslope from the source. The receiver position was varied from zero degrees at the bottom to  $\beta$  at the surface. High resolution plotting was achieved by dividing the y-axis (received angle) into two regions. The first region covers the receiver angles from zero to  $1/5$  of the wedge angle. In this region  $\Delta\delta$  is equal to  $\beta/100$ . The second region covers the remaining wedge angle with  $\Delta\delta$  equal to  $\beta/10$ . This method provides 29 predictions of the pressure amplitude. Another method of plotting carried out was in the region of  $\delta > \beta/2$ ,  $\Delta\delta = \beta/10$ , and in the region of  $\delta < \beta/2$ ,  $\Delta\delta = \beta/100$ . This method provides 54 points to be plotted.

## B. NORMALIZATION

The main goal of this research was to investigate the profile of the pressure amplitude as a function of a number of variables. An example of the numerical values of the pressure amplitude, the normalized pressure amplitude, and the phase at each receiver position is displayed in Appendix C. The sound pressure becomes smaller as the receiver is moved away from the source. If the pressure amplitude were plotted directly, it would be difficult to compare the curves at near distances to the curves at far distances since at the near distances the pressure amplitude is much greater than the pressure amplitude in far distance. Thus, a normalized pressure amplitude is needed. The normalized pressure is obtained as follows: (see Figure 3.1)

We know that the sound pressure at the surface is zero and that the sound pressure is a small number greater than zero at a point near the surface. The first non-zero value of pressure  $P_1$  is at the receiver angle,  $\delta_1 = 98/10$ . We use this first calculated non-zero pressure amplitude as the normalization unit. The normalized pressure is

$$PN = P(\delta)/(P_1) \quad (3.1)$$

where  $P(\delta)$  is the pressure at any point within the wedge.



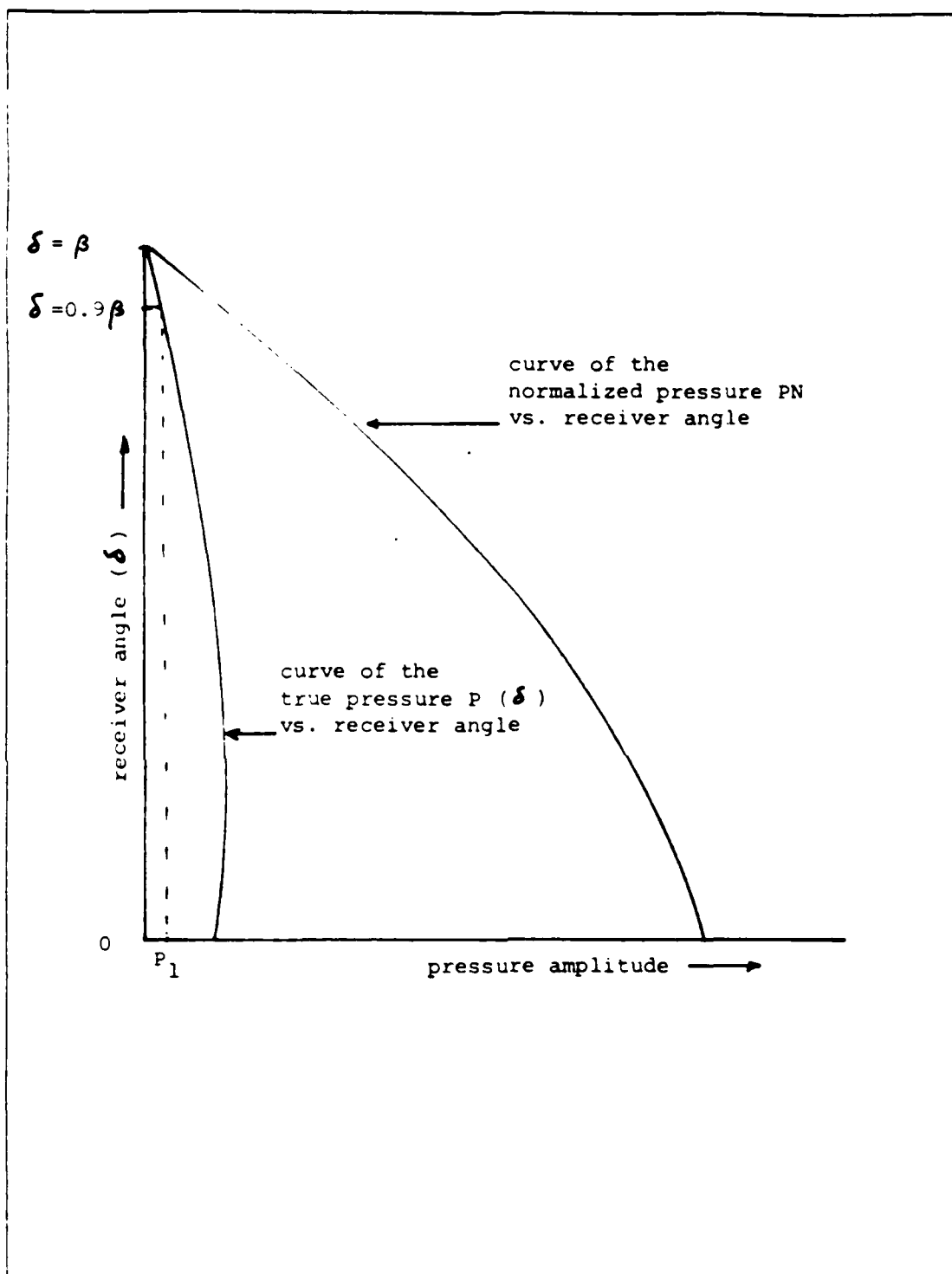


Figure 3.1 Pressure amplitude normalization

### C. PROCEDURE

Figures 3.2 through 3.7 represent the results when the receiver distance and source angle are fixed and the source distance and receiver angle are varied. Figures 3.8 through 3.13 represent the results when the source distance and angle are fixed and the received distance and angle are varied. These cases will be the foundation of our subsequent discussions.

The solid lines indicate the fitted curve and the dots indicate some values of the normalized pressure amplitude. In DSLOW, the dot appears at each third datum.

### D. PROGRAM IMPROVEMENT

DSLOW was designed to provide three-dimensional graphs. For example, the x-axis represents the scaled source distance, the y-axis represents the scaled received distance, and z-axis represents the normalized pressure amplitude. To simplify the presentation, only two-dimensional graphs were presented with the x-axis the normalized pressure amplitude and the y-axis the receiver angle  $\theta$ . All curves are presented with the data fitted with a cubic spline.

The DSLOW program was executed to obtain numerical results of the phase angle, the pressure amplitude, and the normalized pressure amplitude at each receiver position. The first run used double precision for accuracy. Difficulties were encountered when the DISSPLA subprogram

was attached for making the graphical output. When double precision and DISSPLA were not successful, the single precision was used, resulting in round-off error. (See Figure 3.8 at  $R_2 = 10.0$ .)

# RECEIVER ANGLE VS. PRESSURE

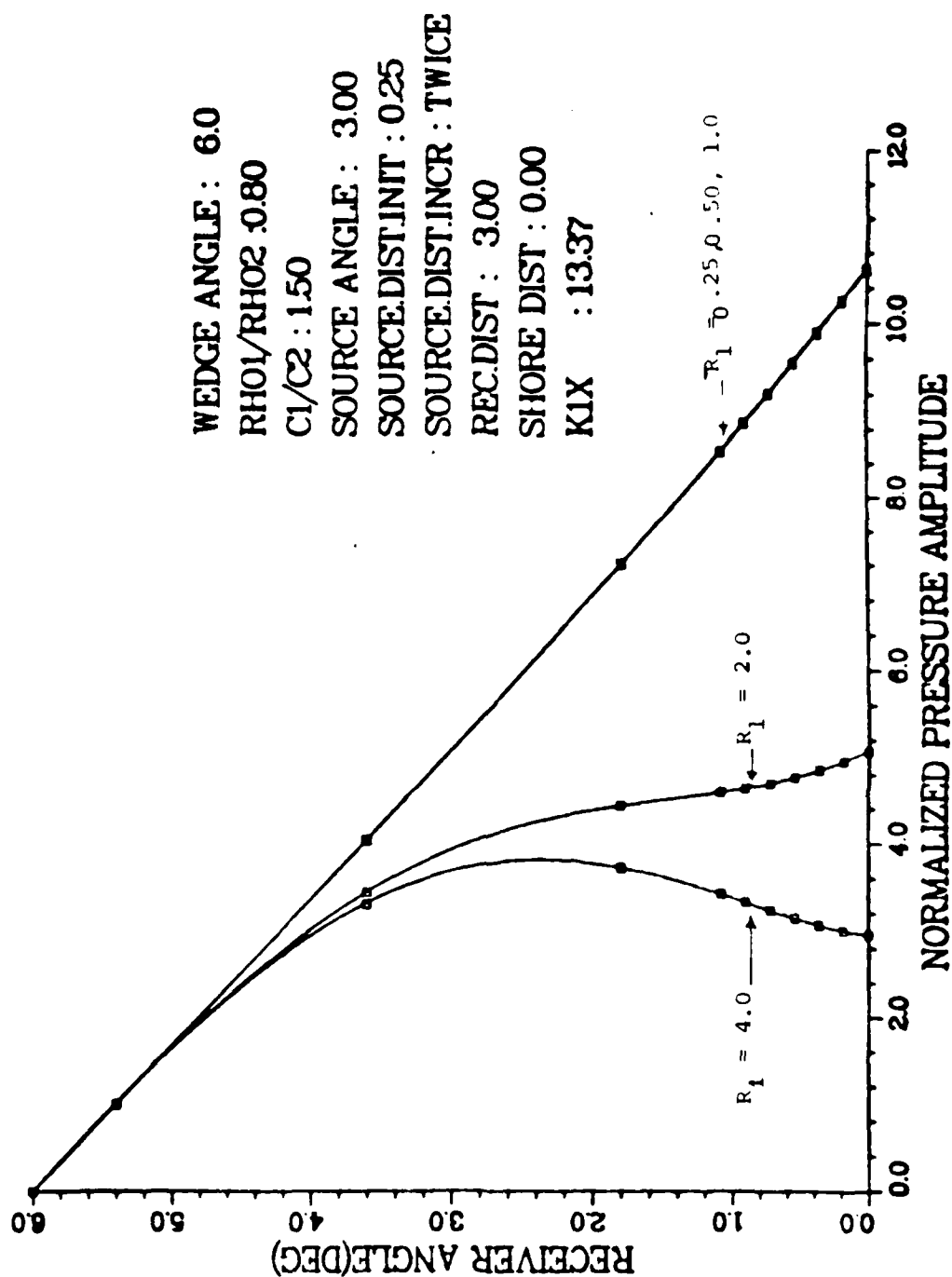


Figure 3.2 Graphs of receiver angle  $\delta$  versus pressure amplitude with  $R_2$  fixed,  $R_1$  varied

# RECEIVER ANGLE VS. PRESSURE

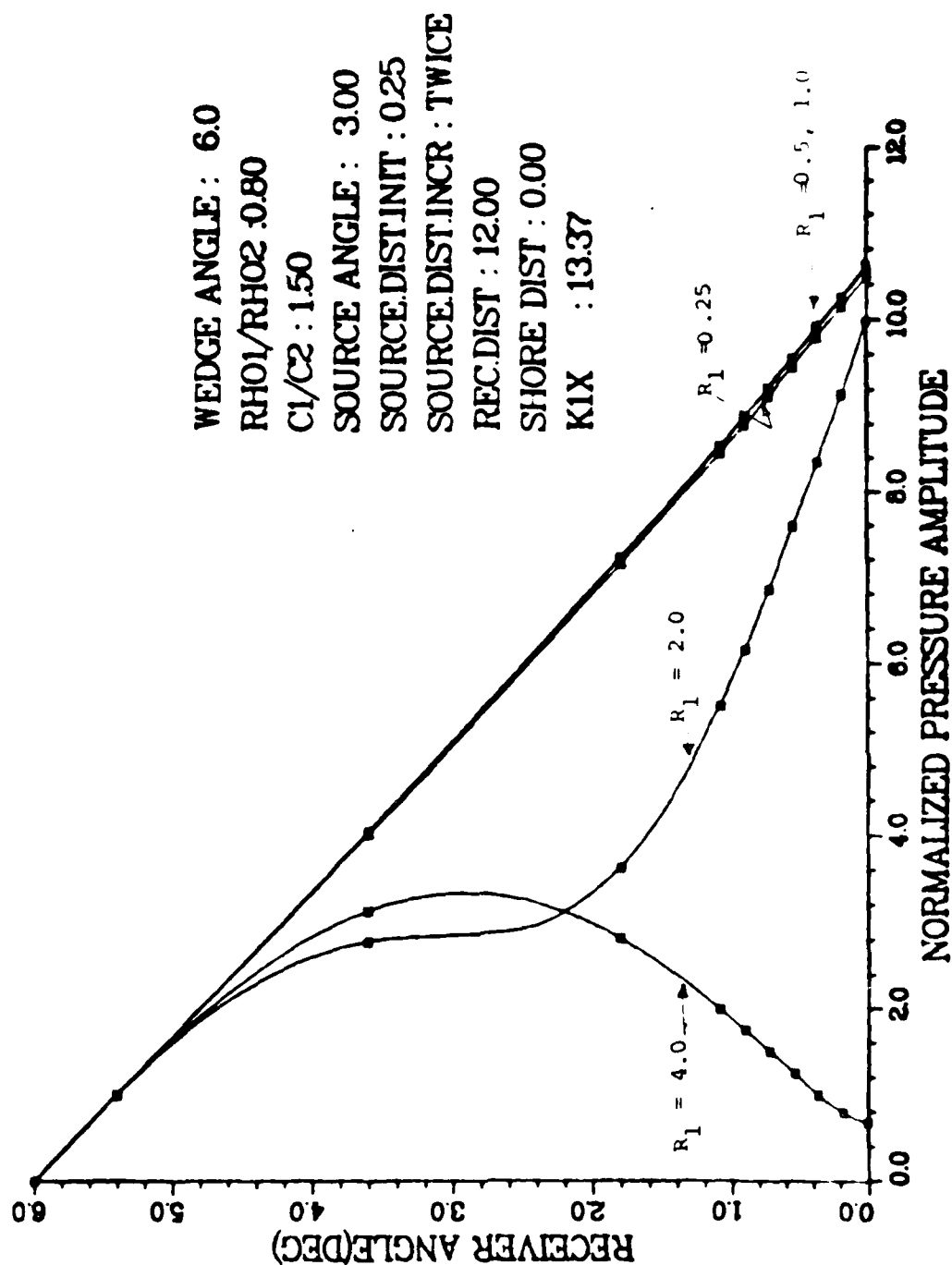


Figure 3.3 Graphs of receiver angle  $\delta$  versus pressure amplitude with  $R_2$  fixed,  $R_1$  varied

# RECEIVER ANGLE VS. PRESSURE

WEDGE ANGLE : 10.0  
 RH01/RH02 : 0.80  
 C1/C2 : 1.10  
 SOURCE ANGLE : 5.00  
 SOURCE.DIST.INIT : 0.25  
 SOURCE.DIST.INCR : TWICE  
 REC.DIST : 3.00  
 SHORE DIST : 0.00  
 K1X : 19.44

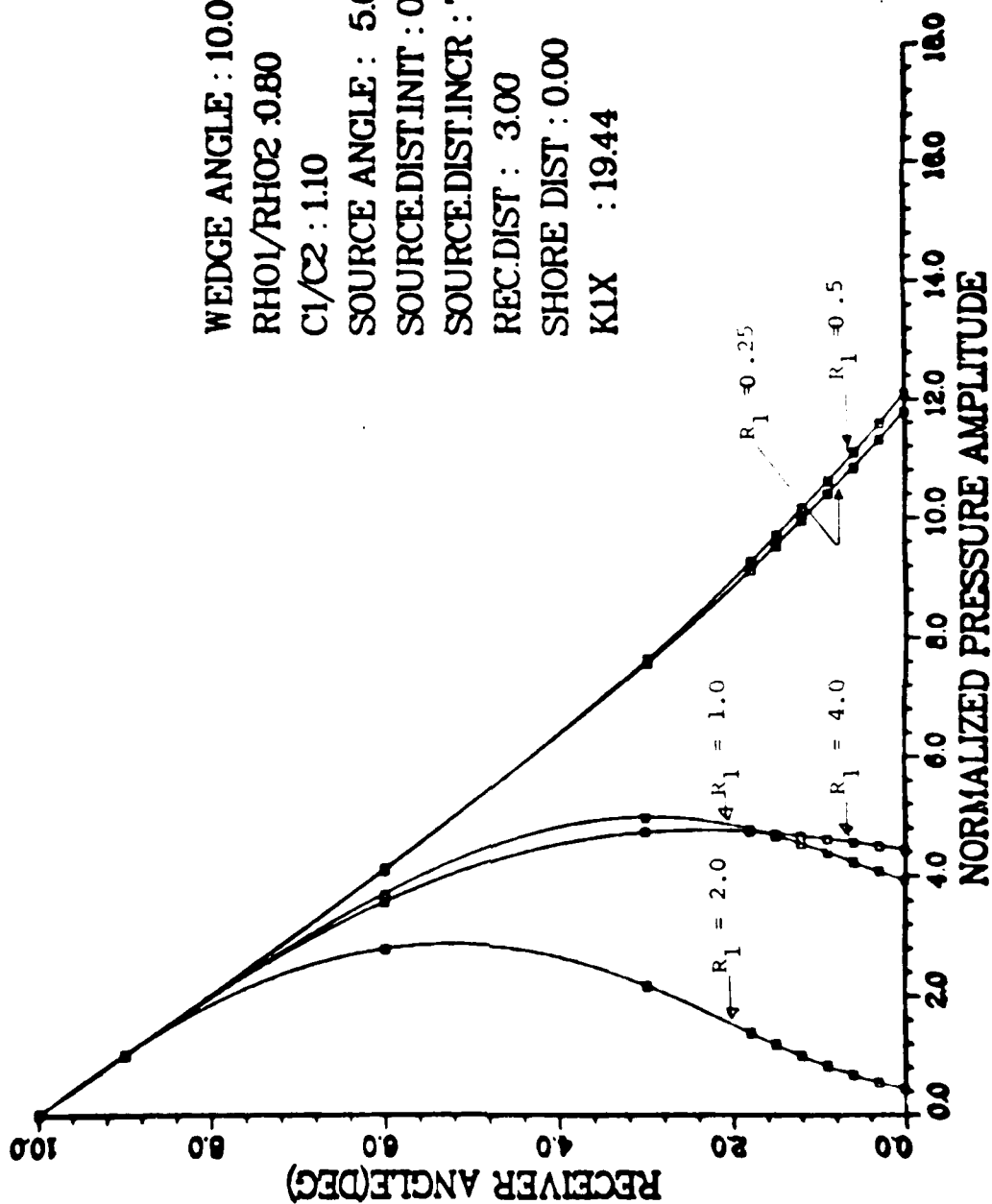


Figure 3.4 Graphs of receiver angle  $\delta$  versus pressure amplitude with  $R_2$  fixed,  $R_1$  varied

# RECEIVER ANGLE VS. PRESSURE

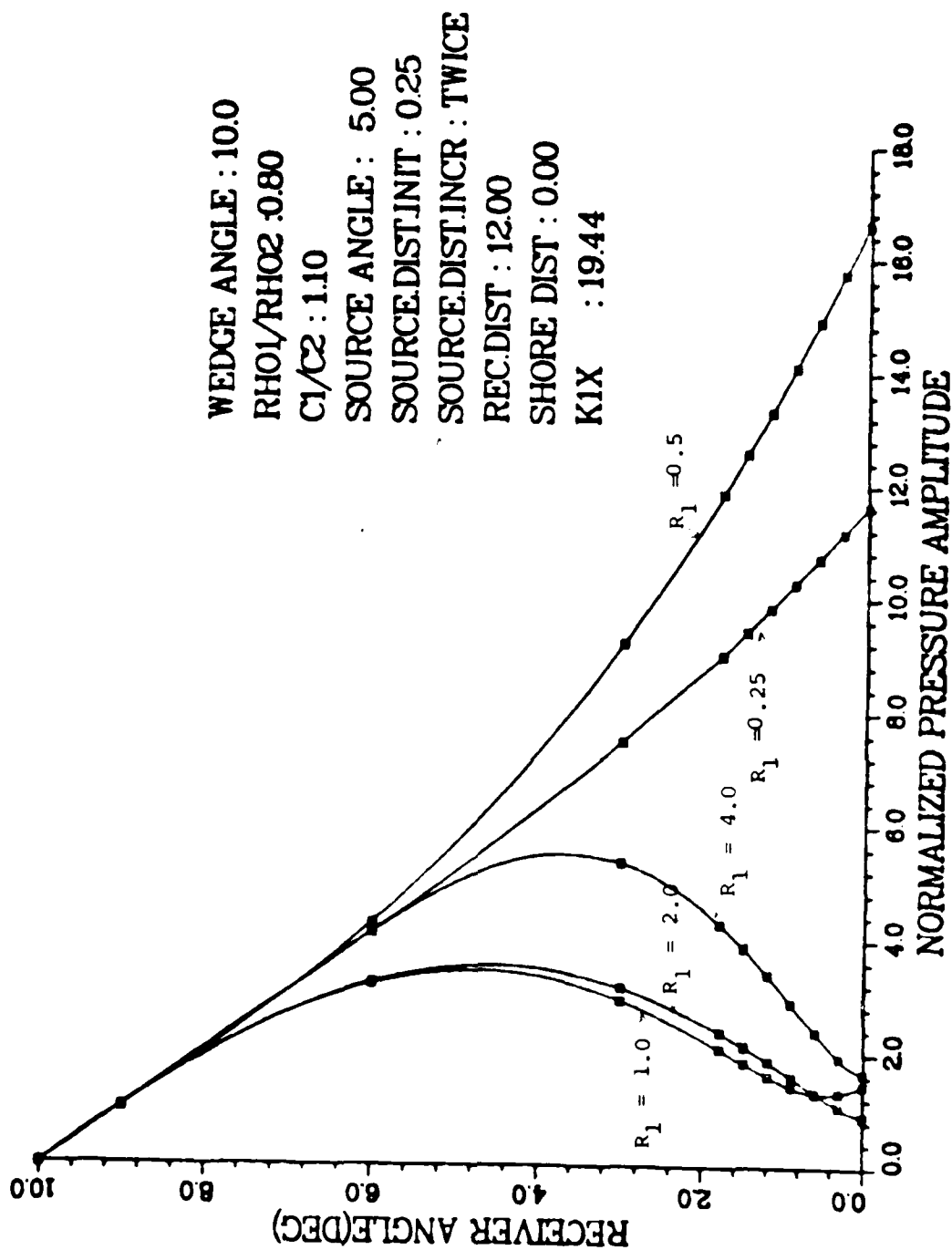


Figure 3.5 Graphs of receiver angle  $\delta$  versus pressure amplitude with  $R_2$  fixed,  $R_1$  varied

# RECEIVER ANGLE VS. PRESSURE

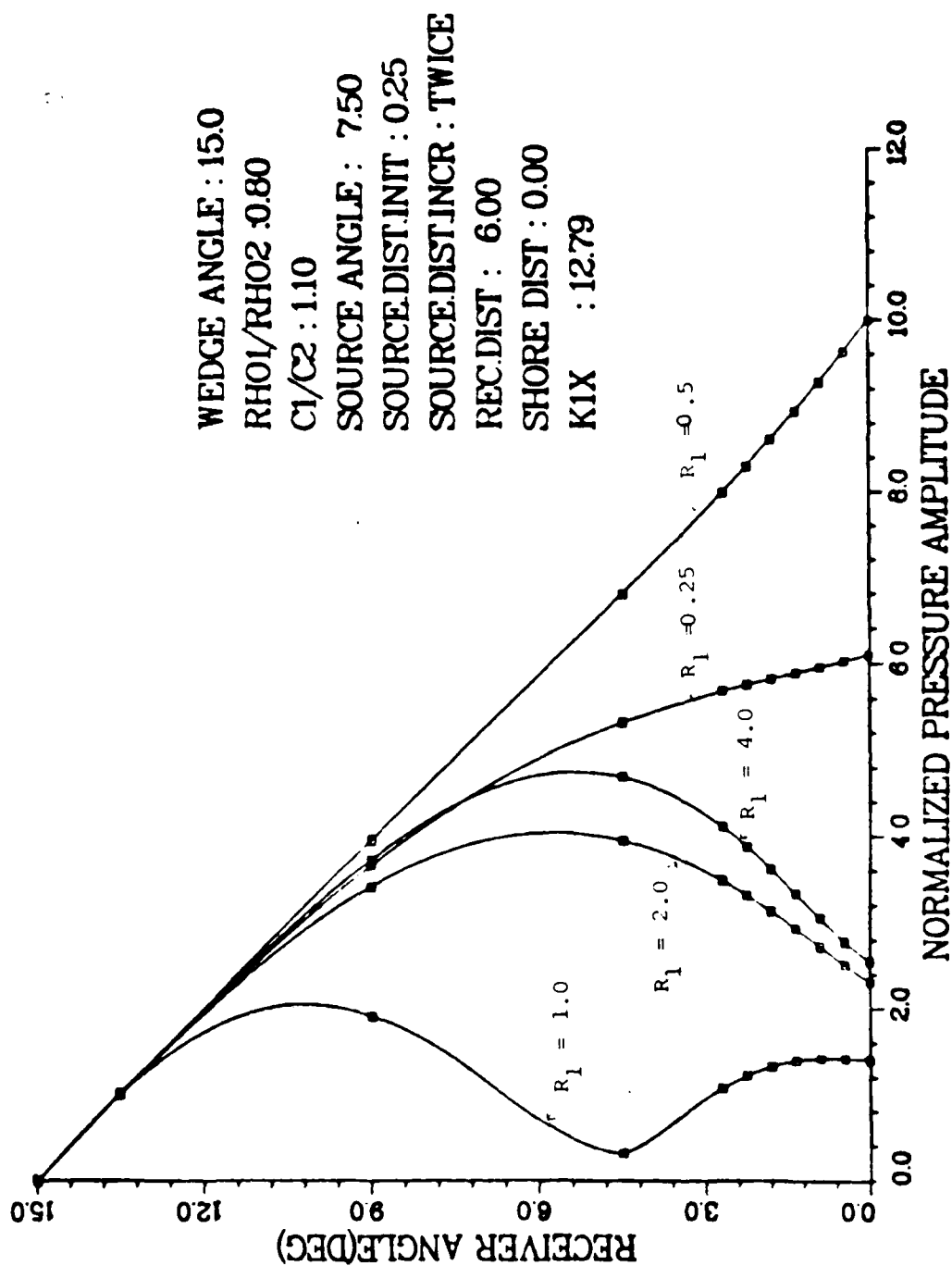


Figure 3.6 Graphs of receiver angle  $\delta$  versus pressure amplitude with  $R_2$  fixed,  $R_1$  varied



# RECEIVER ANGLE VS. PRESSURE

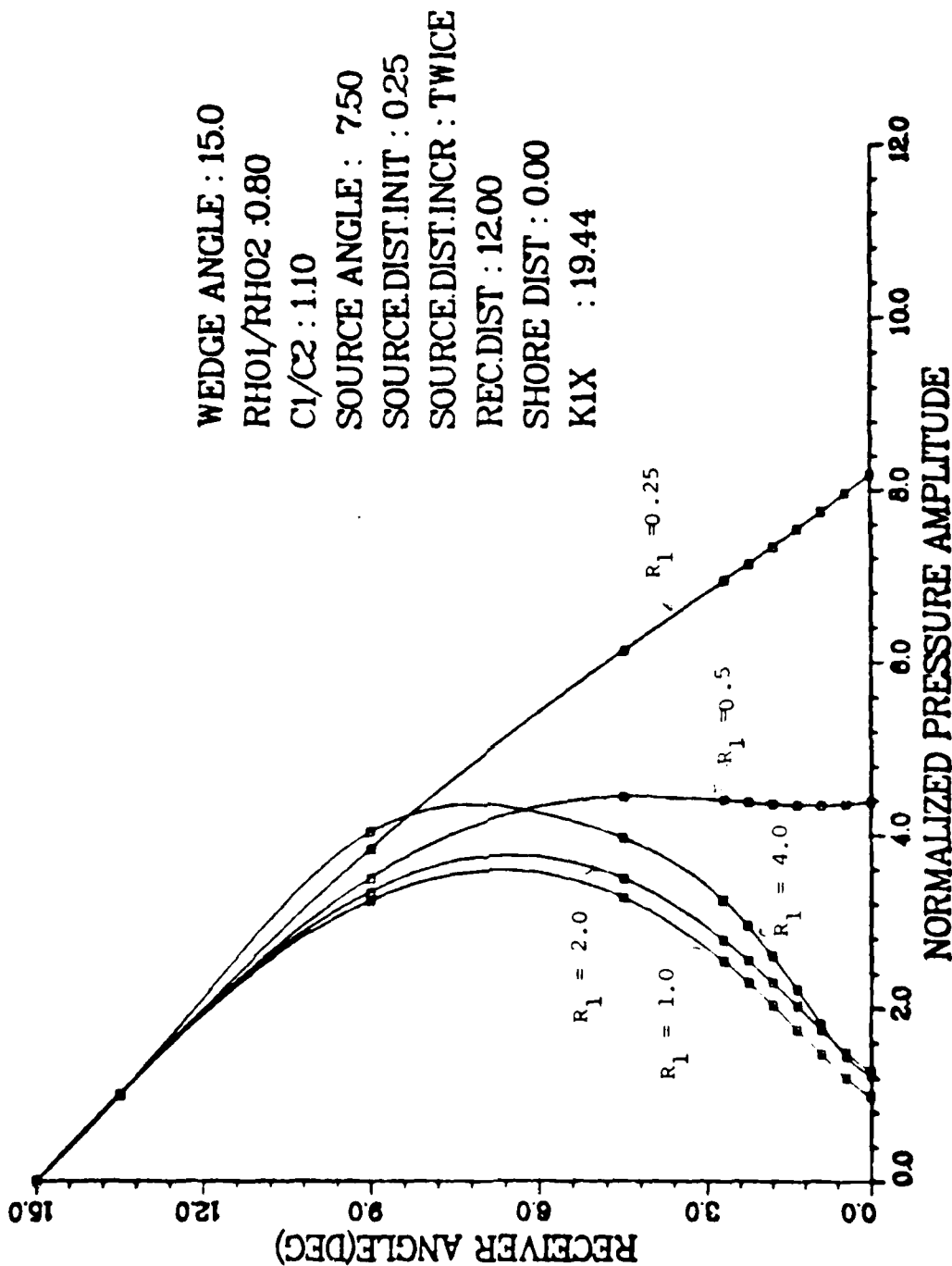


Figure 3.7 Graphs of receiver angle  $\delta$  versus pressure amplitude with  $R_2$  fixed,  $R_1$  varied

# RECEIVER ANGLE VS. PRESSURE

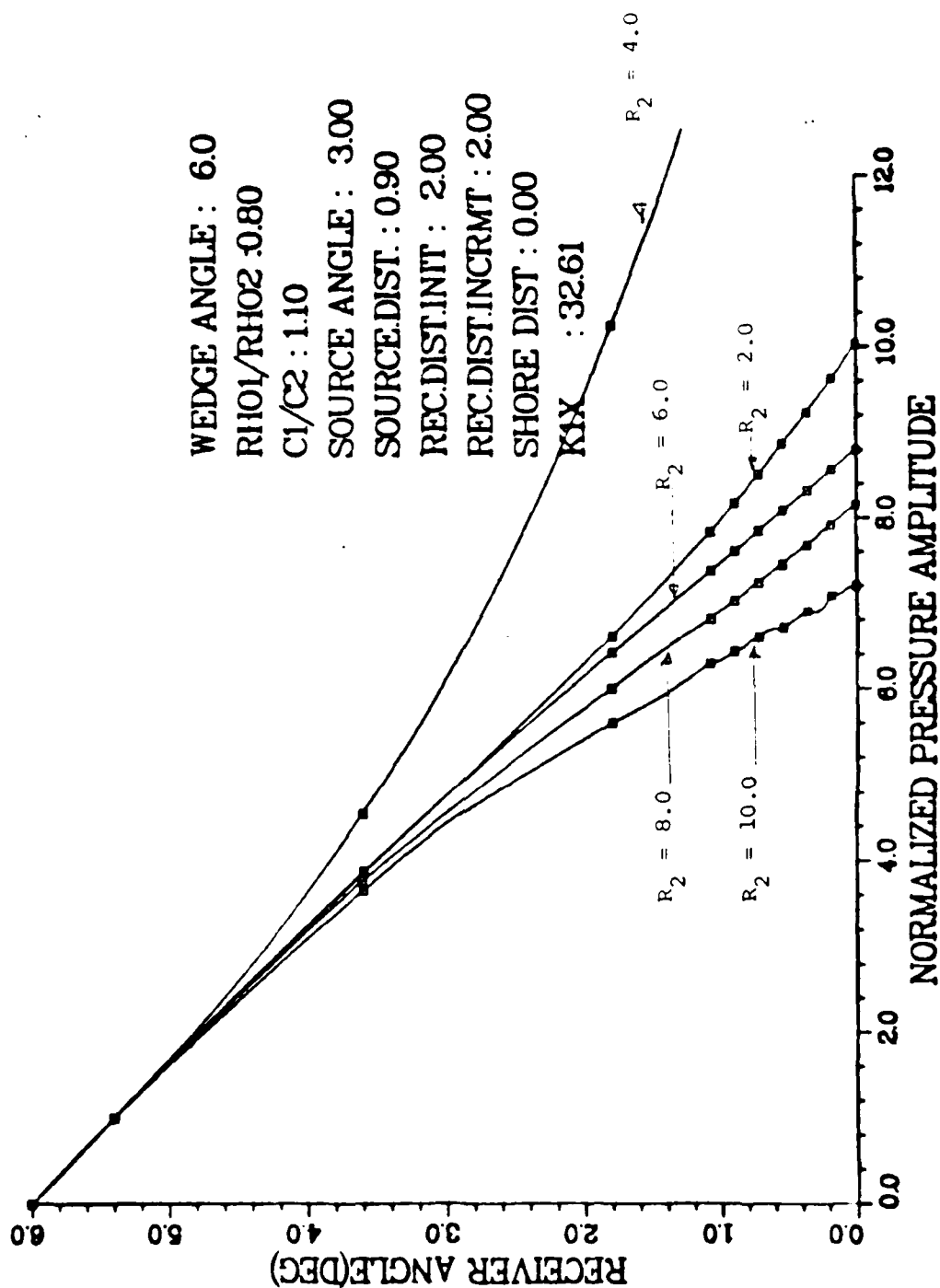


Figure 3.8 Graphs of receiver angle  $\delta$  versus pressure amplitude with  $R_2$  fixed,  $R_1$  varied

# RECEIVER ANGLE VS. PRESSURE

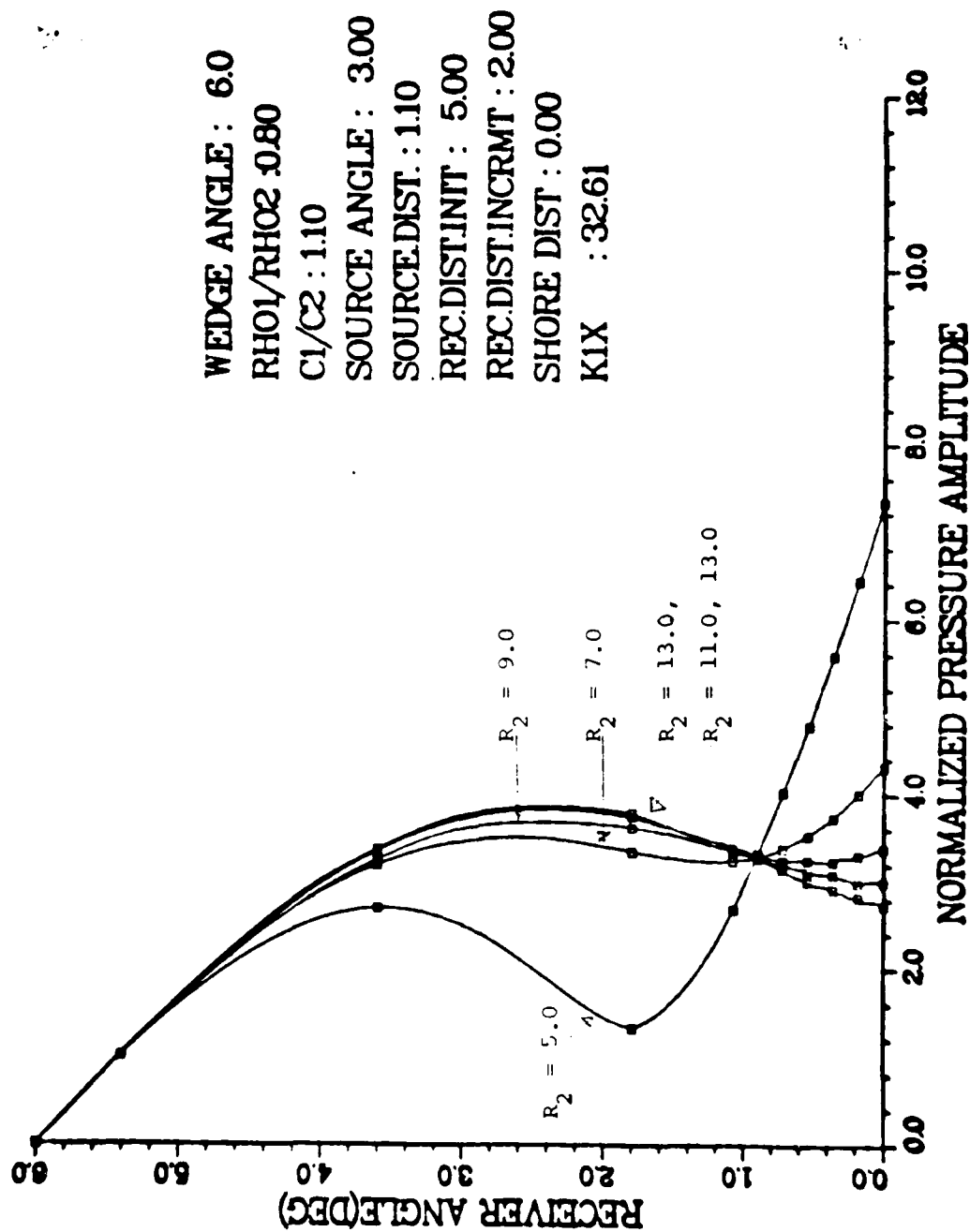


Figure 3.9 Graphs of receiver angle  $\delta$  versus pressure amplitude with  $R_2$  fixed,  $R_1$  varied

# RECEIVER ANGLE VS. PRESSURE

WEDGE ANGLE : 10.0  
 RH01/RH02 : 0.80  
 C1/C2 : 1.10  
 SOURCE ANGLE : 5.00  
 SOURCE DIST. : 1.10  
 REC.DIST.INIT : 2.00  
 REC.DIST.INCRMT : TWICE  
 SHORE DIST : 0.00  
 K1X : 19.44

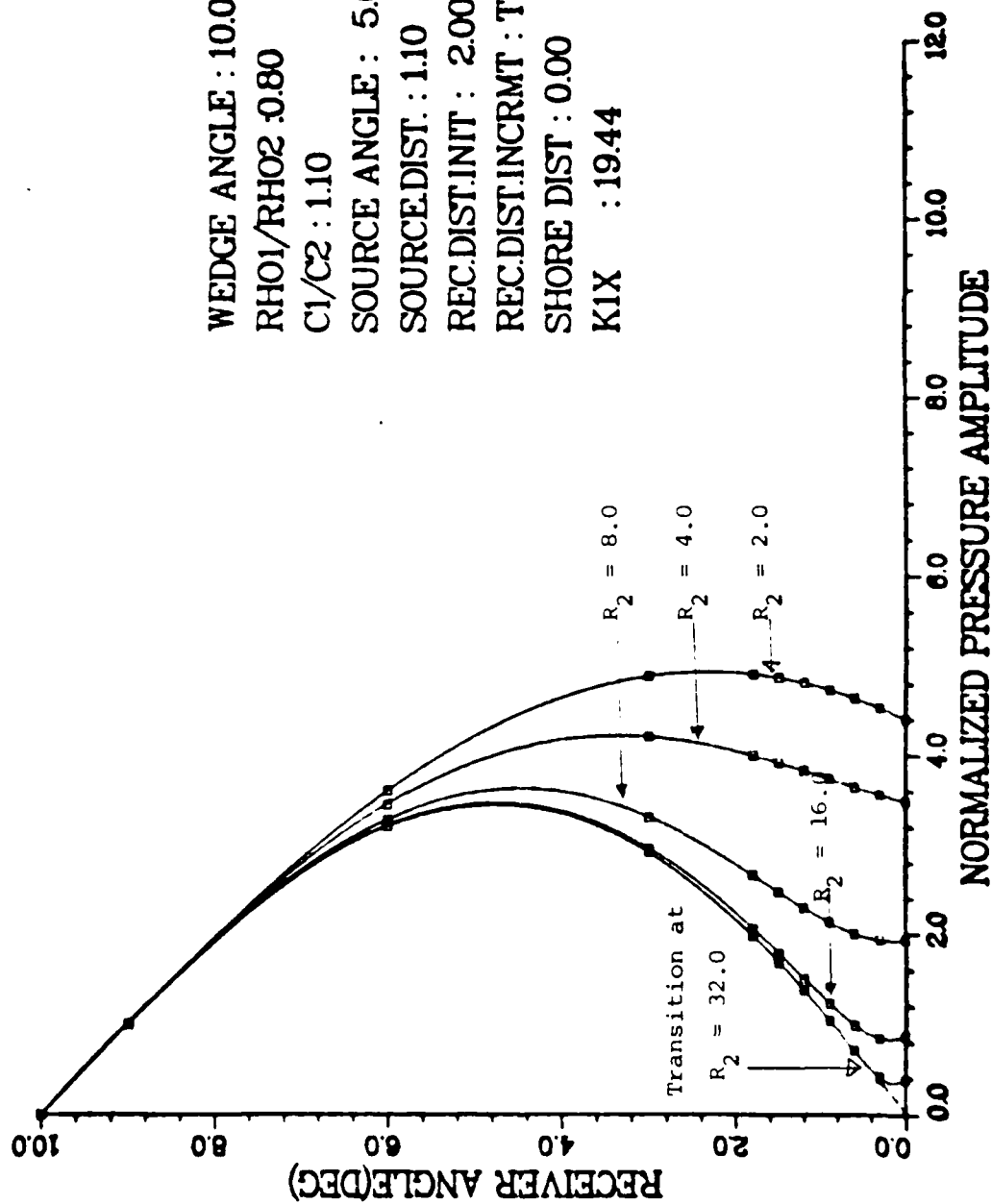


Figure 3.10 Graphs of receiver angle  $\delta$  versus pressure amplitude with  $R_2$  fixed,  $R_1$  varied

# RECEIVER ANGLE VS. PRESSURE

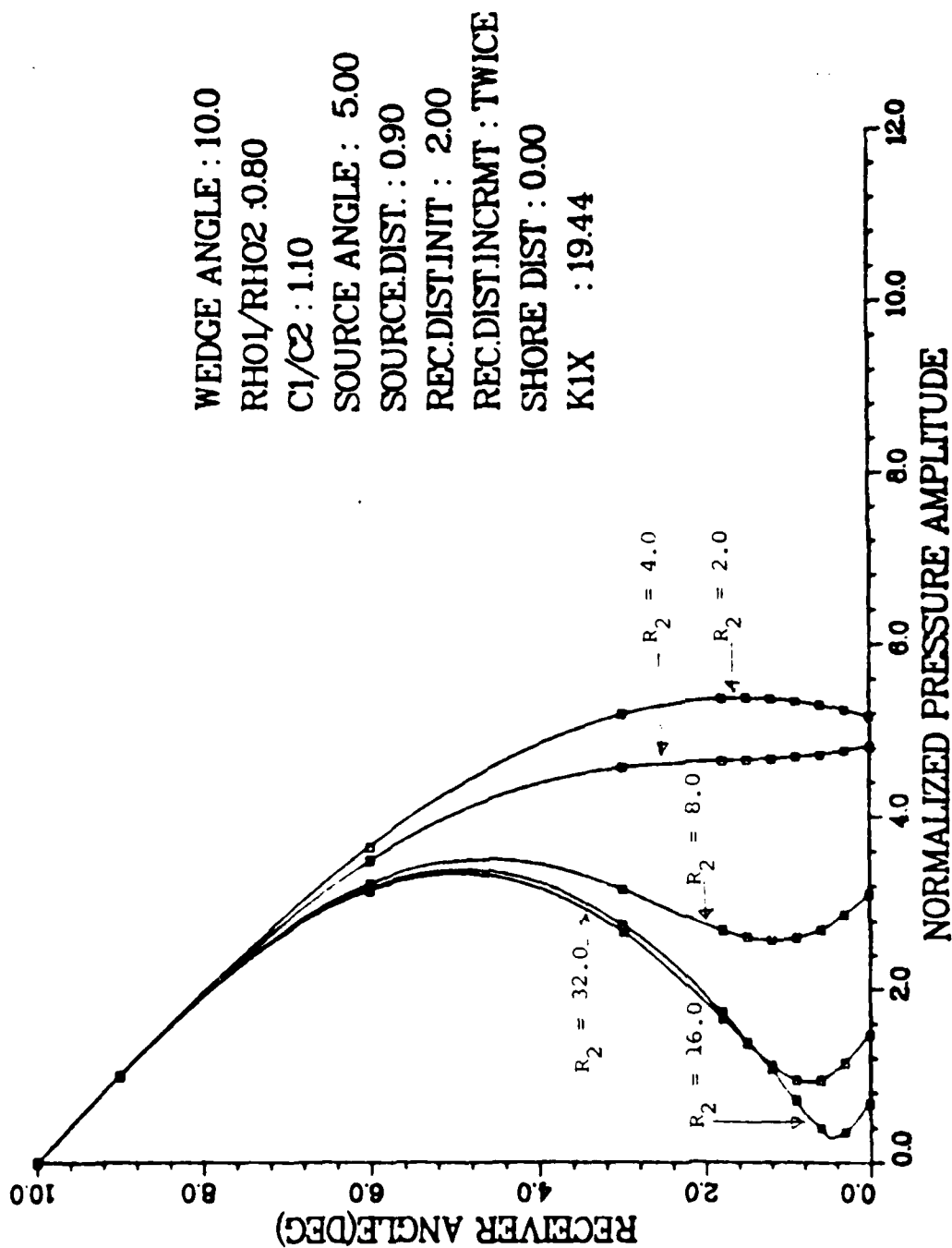


Figure 3.11 Graphs of receiver angle  $\delta$  versus pressure amplitude with  $R_2$  fixed,  $R_1$  varied

# RECEIVER ANGLE VS. PRESSURE

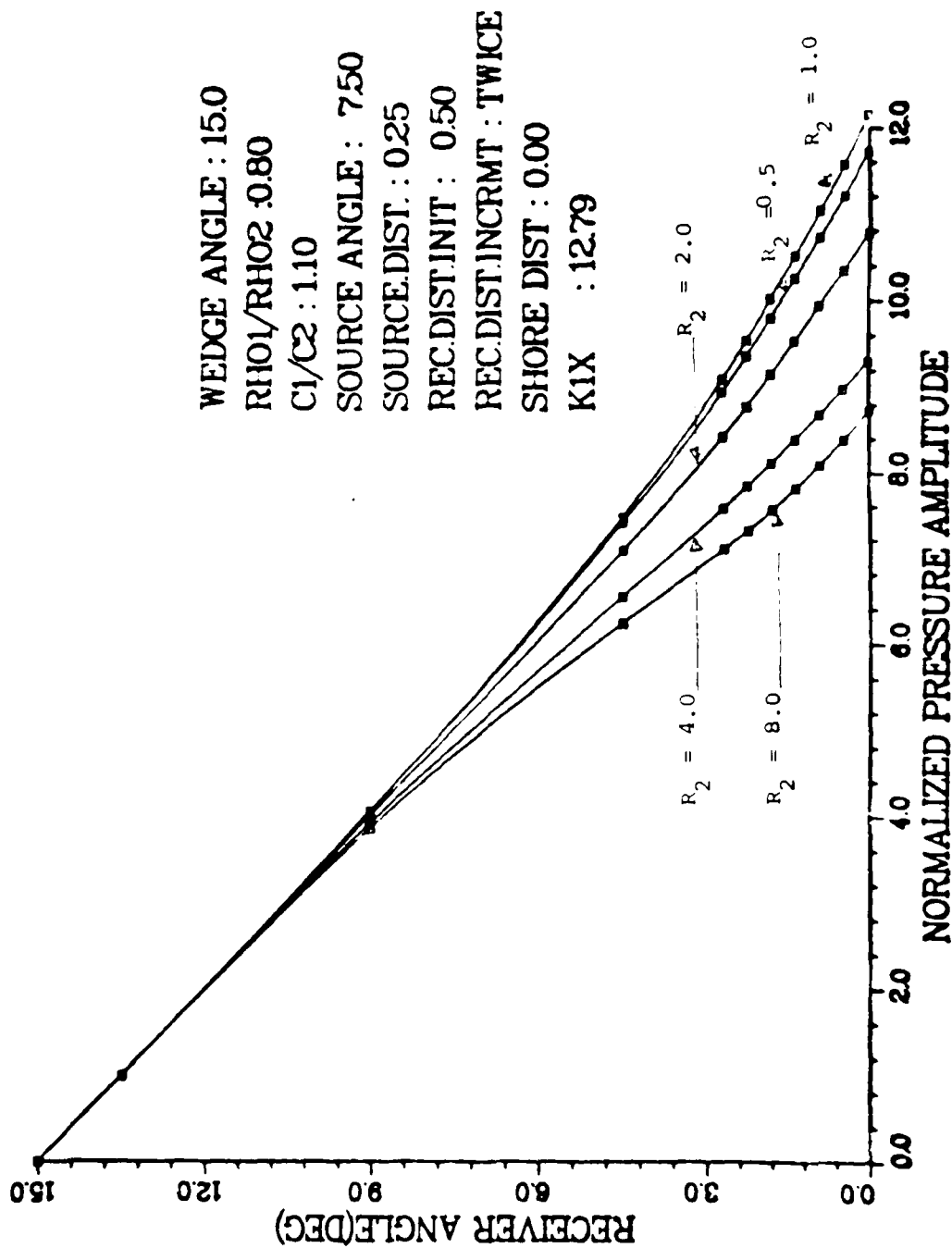


Figure 3.12 Graphs of receiver angle  $\delta$  versus pressure amplitude with  $R_2$  fixed,  $R_1$  varied

# RECEIVER ANGLE VS. PRESSURE

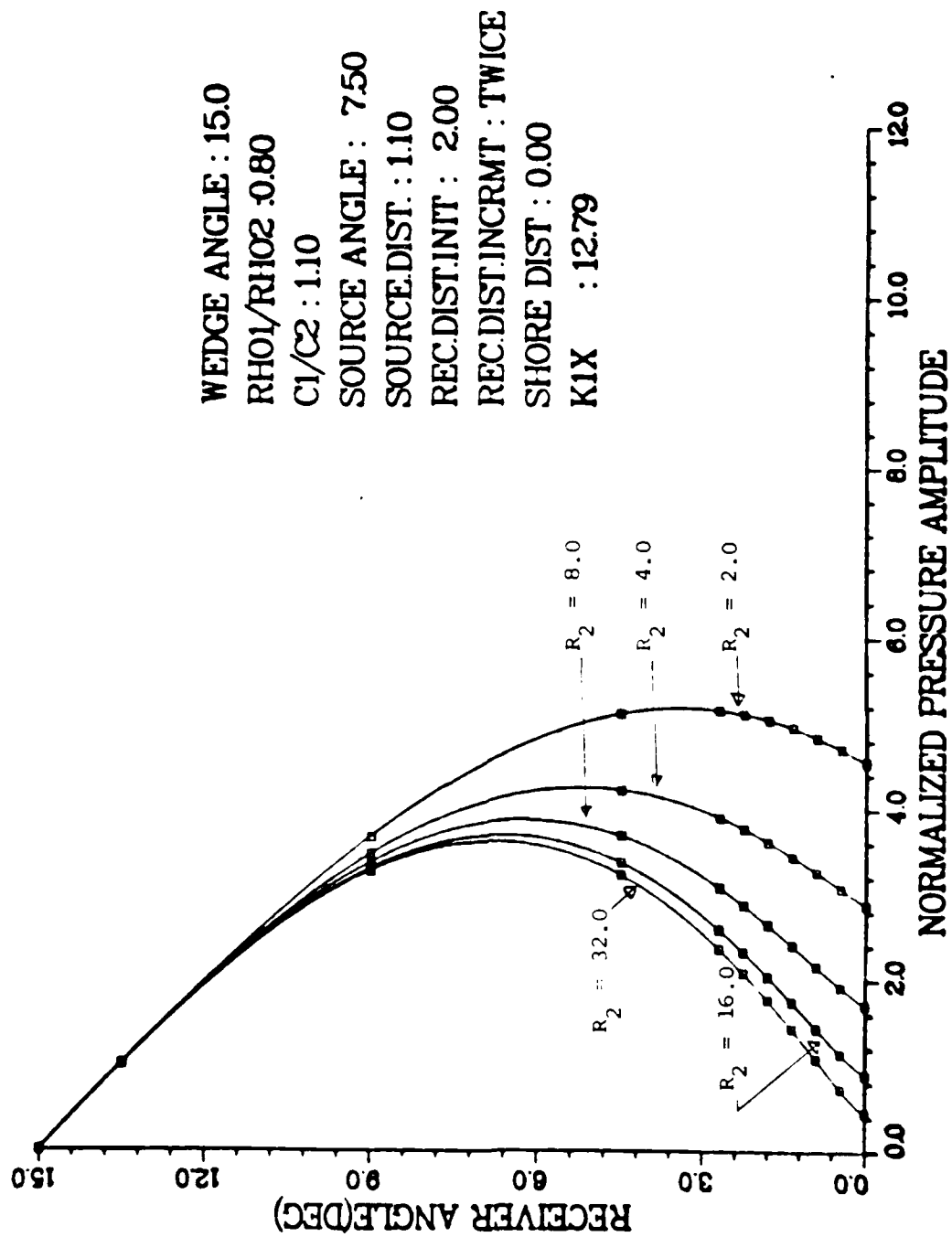


Figure 3.13 Graphs of receiver angle  $\delta$  versus pressure amplitude with  $R_2$  fixed,  $R_1$  varied

#### IV. DISCUSSIONS

##### A. GRAPHICAL OUTPUT

The graphs of normalized pressure amplitude as a function of receiver angle  $\delta$  were investigated for various source distances  $R_1$  and receiver distances  $R_2$  (Fig. 3.2 to 3.13) while the other parameters are held constant. For a given wedge angle  $\beta$  and sufficiently small source distance (Fig. 3.8 and 3.12), at all receiver distances, the pressure increases uniformly towards the bottom. For greater source distances, (Fig. 3.9 -3.11) the pressure attains a maximum within the wedge for all receiver distance.

As the receiver distance is increased (Fig. 3.9), a pressure minimum develops between the maximum and the bottom. An important property of the curves of pressure versus receiver angle when there is a maximum and minimum is that, at a specific receiver distance, the pressure above the minimum can be extrapolated to zero pressure on the bottom. (See Fig. 3.10 with  $R_2 = 32$ .) This receiver distance is called the "transition point." So far, we do not know the properties of the transition point. We use the transition point for indicating the behavior of the curves when the parameter involved is varied. The transition point appeared twice in some cases, but in the following discussions the first transition point is the only point we



will be concerned with. (See Fig. 4.1 for transitions correspond to  $R_2 = 4.6$  and  $6.4$ .)

## B. GRAPHS CLASSIFICATION

The development of curves with the source distance ( $R_1$ ) and the receiver distance ( $R_2$ ) as variables was observed. As  $R_1$  or  $R_2$  are varied the curve changes from a linear curve to a curve with an observable minimum (Fig. 3.9,  $R_2 = 5.0$ ) and finally to a curve without a minimum (Fig. 3.9,  $R_2 = 9.0$ ). Three different types of curves resulted from the series of two-dimensional plotting. They are described below:

### 1. Type 1 Curves

Type 1 curves (Fig. 4.2) are those where the sound pressure is equal to zero at the surface and maximum at the bottom and is almost linearly dependent on depth. These curves are most pronounced when the source distance is much smaller than the characteristic distance. The closer the source is to the characteristic distance, the more nonlinear the curves (Figs. 3.3 and 3.4).

### 2. Type 2 Curves

Type 2 curves (Fig. 4.3) are those where the sound pressure is zero at the surface, maximum somewhere between the surface and the bottom with no minimum. These types of curves are generated when the source is placed at a point much greater than the characteristic distance. Type 2

# RECEIVER ANGLE VS. PRESSURE

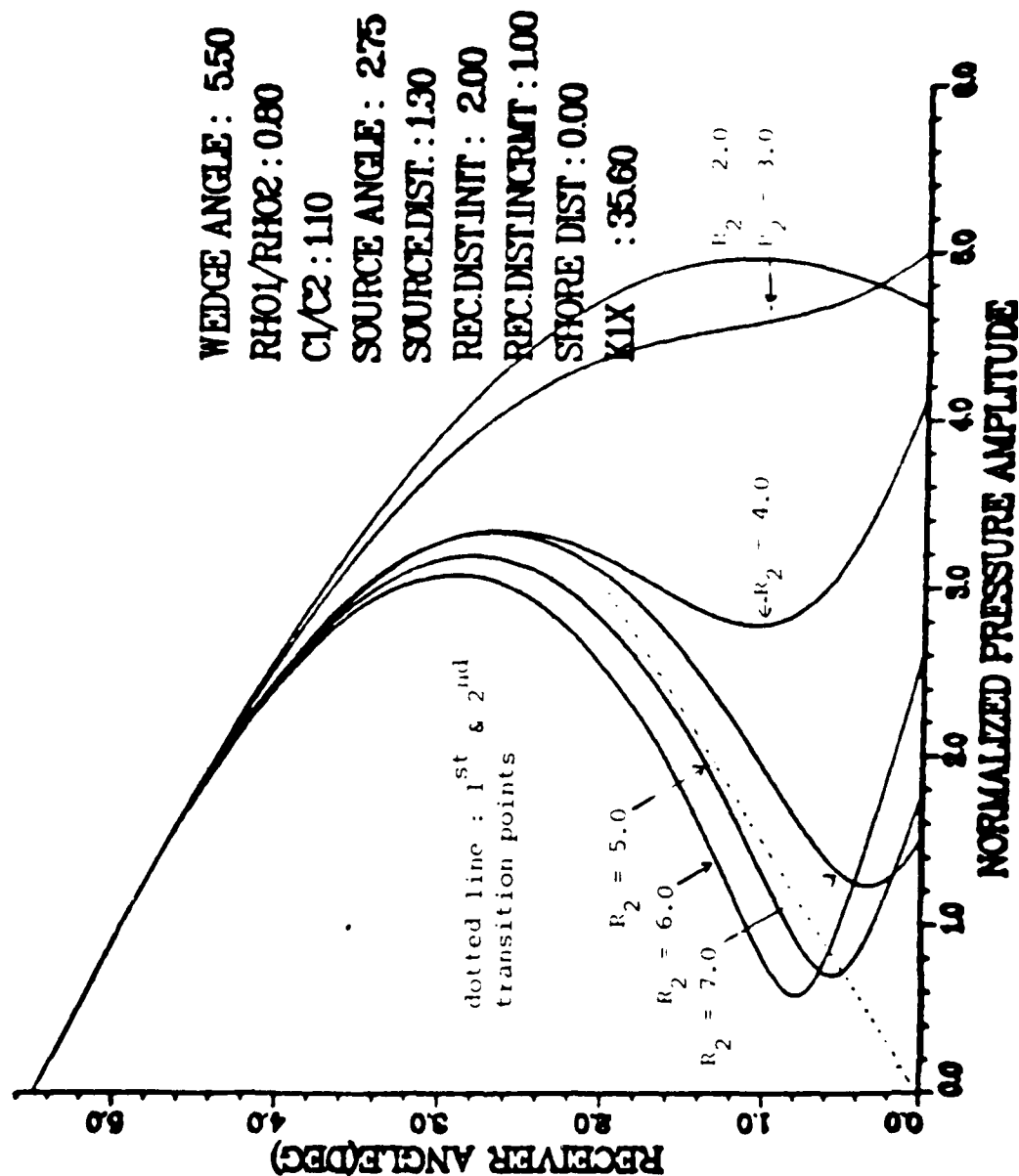


Figure 4.1 The plots where there are two transition points,  $R_2=4.6$  is the first and  $R_2=6.4$  is the second

curves indicate that the sound energy in the wedge is well collimated and that reflection is negligible.

### 3. Type 3 Curves

Type 3 curves (Fig. 4.4) are those that have a minimum pressure. These curves occur when the source is a distance slightly greater than, or less than, the characteristic distance. Tables 1, 2, and 3 of Appendix D show the receiver positions at the first transition points. Three different values of  $\beta$ , two different values of  $\rho_1/\rho_2$ , and two different values of  $c_1/c_2$  were used in making these tables. The transition point did not occur when  $\beta = 15^\circ$ ,  $\rho_1/\rho_2 = 0.90$ ,  $c_1/c_2 = 1.10$ . An explanation can be offered using the fact that for these particular sound-speed and density ratios an angle of intromission exists [Ref. 15]. Since the angle of intromission is the grazing angle at which the sound energy is completely transmitted into the slow bottom, it is plausible that no transition point occurs.

### C. TRANSITION POINT

By varying the wedge angle  $\beta$  in small increments  $\Delta\beta = 0.5^\circ$  starting with  $\beta = 5^\circ$ , and ending at  $\beta = 7^\circ$ , it was found that transition occurs for source distances within the range from 1.0 to 1.5.

For  $R_1 < 1.0$ , no transition point was observed; the curves are the Type 1. For  $1.0 < R_1 < 1.5$ , the evolution of

curves as the receiver distance varied can be explained as follows: first, the receiver is placed near the source and gradually it is shifted further from the source. The minimum in the pressure decreases reaching the point where the curves extrapolate to zero (the first transition point). Further detailed observations were made on this particular facet by varying the source distance and the receiver distances. The results of these observations are tabulated and graphed in Appendices D and E. When the receiver is moved away from the source, the minimum will reach a minimum pressure then the pressure increases until it reaches the point where the curves again can be extrapolated to zero, this is the second transition point (See Fig. 4.1).

For  $P_1 > 1.5$ , there will be no transition point. The curves are the Type 2.

The transition point as a function of source angle can be observed using the tables in Appendix D. In most cases the greater the source angle  $\gamma$ , the closer the transition point is to the apex. Graphs of transition point as a function of  $R_1$  (Appendix E) indicate that the smaller  $\beta$  the more regular the curves. This is easy to understand because the smaller  $\beta$ , the more accurate the observation of transition point; the greater  $\beta$  the less accurate the data.

# RECEIVER ANGLE VS. PRESSURE

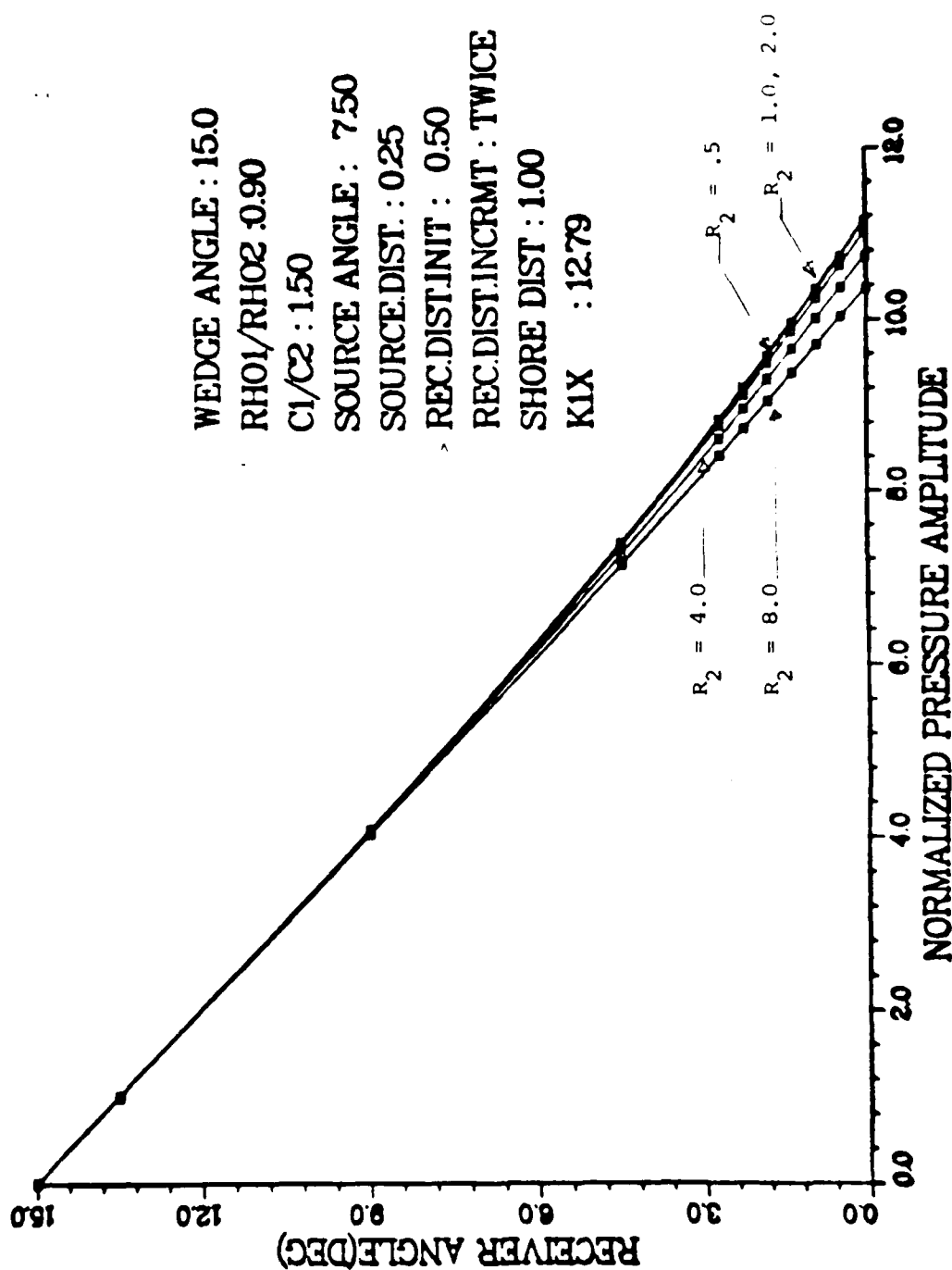


Figure 4.2 Type 2 curves, indicating a pressure amplitude nearly linear with depth

# RECEIVER ANGLE VS. PRESSURE

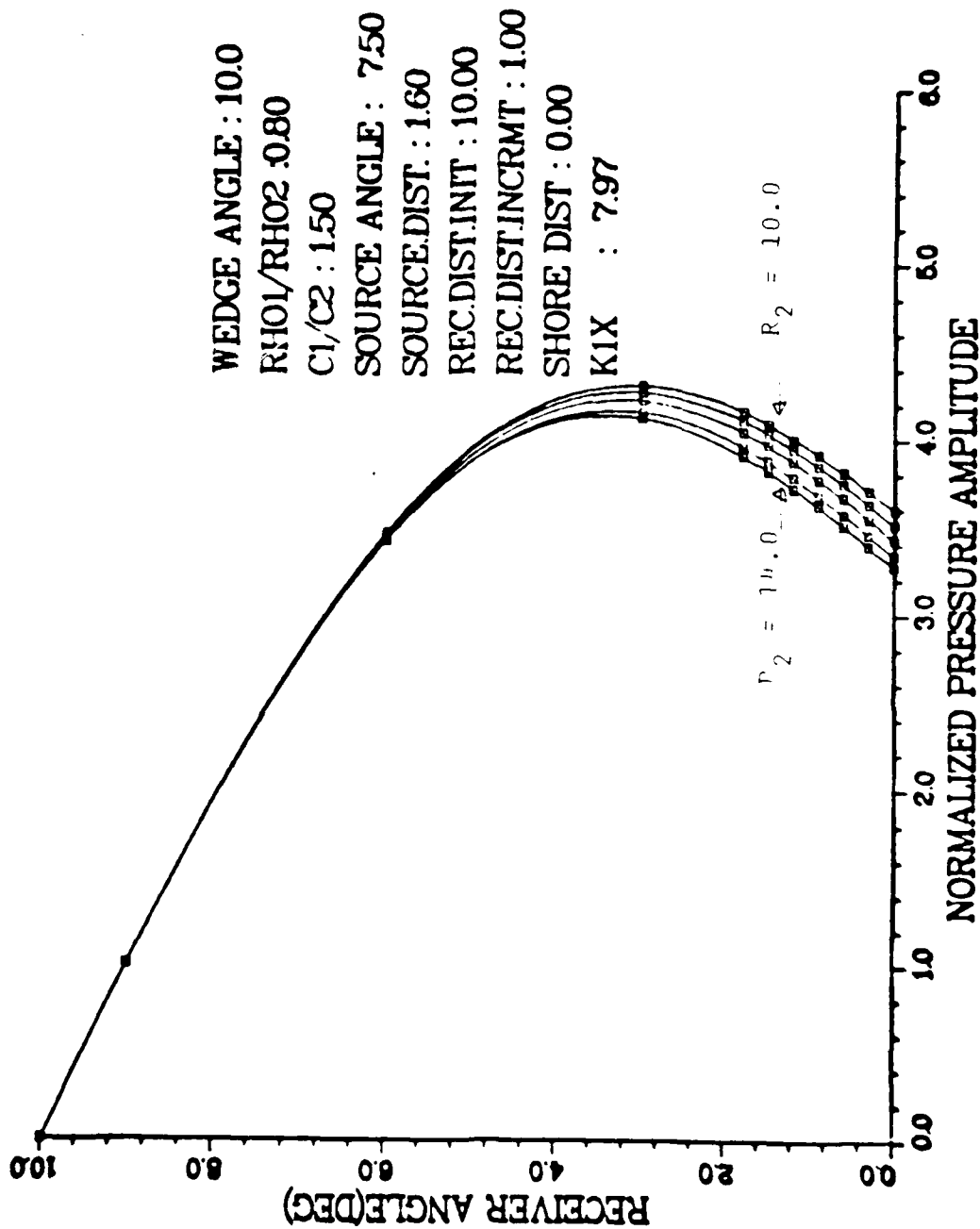


Figure 4.3 Type 2 curves, indicating a well-collimated sound field as the source away from the apex

# RECEIVER ANGLE VS. PRESSURE

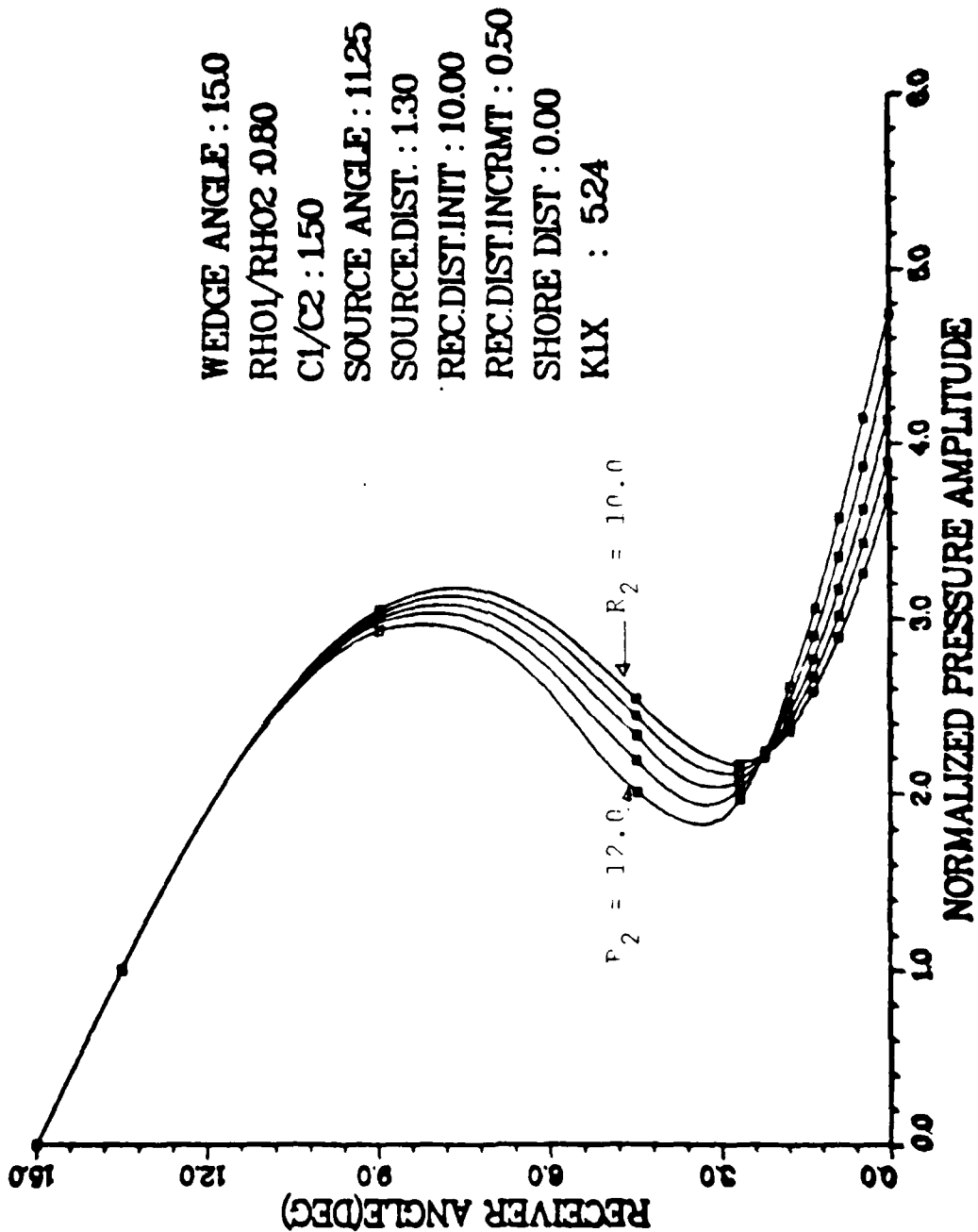


Figure 4.4 Type 3 curves, indicates the presence of reflection and refraction near the bottom

#### D. PARAMETER VARIATIONS

Variation of parameters was done by changing one parameter of interest while all others were held constant, for fixed source and receiver distances, and plotting the receiver angle versus normalized pressure amplitude.

The parameters  $\beta$ ,  $\rho_1/\rho_2$ , and  $c_1/c_2$ , were held constant and the pressure amplitude was plotted for various  $\beta$ ,  $R_1$ , and  $R_2$ . The  $\gamma$ 's are set at  $\beta/4$ ,  $\beta/2$ , and  $3\beta/4$ . Variations in the shore distance ( $Y_0$ ) can be made because the program is available, but to simplify the investigation,  $Y_0$  was set equal to zero for all plots (Fig 4.2 is included as an example for  $Y_0 \neq 0$ ).

##### 1. Variations of $\beta$

Initially, the values of  $\beta$  investigated were:  $6^\circ$ ,  $10^\circ$ , and  $15^\circ$ . The major effect created by altering the value of  $\beta$  is that, for the same values of  $R_1$ ,  $\rho_1/\rho_2$ , and  $c_1/c_2$ , the smaller  $\beta$ , the shorter the transition point (see Figs. 3.9 and 3.10, Tables 1, 2, and 3 of Appendix D).

##### 2. Variations of $\gamma$

The variations of  $\gamma$  from  $\gamma = \beta/4$  (the source is placed near the bottom) to  $\gamma = 3\beta/4$  (the source is placed near the surface) are presented in Tables 1, 2, and 3 indicating that the greater  $\gamma$  the shorter the transition point. It is not always true, for instance in Table 1 at  $\beta = 6^\circ$ ,  $R_1 = 1.50$ , the greater  $\gamma$  the longer transition point, for the



rises. (See Appendix D.)

3. Variations of  $c_1/c_2$  and  $\rho_1/\rho_2$

Variations of the acoustical parameters  $c_1/c_2$  and  $\rho_1/\rho_2$  were done, but did not give a significant variation of the sound pressure profile.

## V. CONCLUSIONS AND RECOMMENDATIONS

### A. CONCLUSIONS

The program DSLOW gives good plots representative of the sound energy distribution within the wedge. The sound energy can be well collimated by the wedge. This phenomenon is strongly affected by the source position. At a source position close enough to the apex, sound energy is distributed linearly with respect to the depth. As the source moved away from the apex, the distribution of sound energy becomes more complex. Sometimes a minimum is found; this minimum may be caused by the presence of sound energy reflected by the bottom.

The source position plays a major role in forming the pressure distribution profile. The pressure distribution is also very sensitive to the parameter variation at small source distances, but it becomes insensitive at large source distance. The characteristic distance must have physical meanings rather than just an arbitrary number, because when the source distance is in proximity to the characteristic distance, the model is most sensitive.

The model is restricted when the single precision mode generates round-off error and rough curves which do not allow for accurate analysis.

## B. RECOMMENDATIONS

1. Single precision produces good results, but failed in some cases. Double precision would improve the program, but increase the execution time. This must be done by running the program in double precision, and accumulating the result in single precision before plotting the data by DISSPLA.
2. It is suggested that the program be run using more realistic parameters and observing the effects on the characteristic distance and transition point.
3. Further study validating DSLOW in comparison with experimental results is suggested.

## APPENDIX A DSLOW ALGORITHM

The pressure amplitude calculation

$$N_1 = \text{INT}[180 \beta] \quad (\text{eqn A.1})$$

$$K_1 X = \frac{\pi}{2 \tan \beta \tan[\arccos(c_2/c_1)]} \quad (\text{eqn A.2})$$

$$AL = \alpha K_2 = 0.0001 \quad (\text{constant}) \quad (\text{eqn A.3})$$

$$D_2 = Y_0^2 + R_1^2 + R_2^2 \quad (\text{eqn A.4})$$

$$R_3 = 2R_1 R_2 \quad (\text{eqn A.5})$$

$$R_8 = \sqrt{D_2 - R_3 \cos[(N-1)\beta + \gamma - \delta]} \quad (\text{eqn A.6})$$

$$R_9 = \sqrt{D_2 - R_3 \cos[(N-1)\beta + \gamma + \delta]} \quad (\text{eqn A.7})$$

$$S_2 = (-1)^{\text{INT}(N_1/2)} \quad (\text{eqn A.8})$$

$$W_1 = 2AL(c_1/c_2)^2 \quad (\text{eqn A.9})$$

$$SI = \{ [R_1 \sin[(N-1)\beta + \gamma] - 2[\text{INT}((N-1)/2)\beta + R_2 \sin[2\text{INT}((N-1)/2)\beta - \delta]] \} R_8 \quad (\text{eqn A.10})$$

$$CI = \sqrt{(1-SI^2)} \quad (\text{eqn A.11})$$

$$T = SI/D_1 \quad (\text{eqn A.12})$$

$$W_0 = (-c_2 + c_1/c_2) \quad (\text{eqn A.13})$$

$$Y = \sqrt{W_0^2 + W_1^2} \quad (\text{eqn A.14})$$

$$Z = |W_0| \quad (\text{eqn A.15})$$

$$Y_1 = \sqrt{(Y + W_0)^2} \quad (\text{eqn A.16})$$

$$Y_2 = \sqrt{(Y - W_0)^2} \quad (\text{eqn A.17})$$

$$Z_1 = \frac{T_1 \cdot Y_2}{(T \cdot Y_2)^2 + Y_1^2} \quad (\text{eqn A.18})$$

$$Z_2 = \frac{Y_1}{(T \cdot Y_2)^2 + Y_1^2} \quad (\text{eqn A.19})$$

$$Z_5 = \frac{(T^2 \cdot Y_2)^2 - Y_1^2}{(T^2 \cdot Y_2)^2 + Y_1^2} \quad (\text{eqn A.20})$$

$$Z_6 = \frac{2Y_1 T}{(T^2 \cdot Y_2)^2 + Y_1^2} \quad (\text{eqn A.21})$$

$$P_1 = \sum_{n=1}^{N_1} (-1)^{\text{INT}(N/2)} \{Z_5 \cos(R_{8n} K_1 X) + Z_6 \sin(R_{8n} K_1 X)\} R_{8n} \quad (\text{eqn A.22})$$

$$P_2 = \sum_{n=1}^{N_1} (-1)^{\text{INT}(N/2)} \{-Z_5 \sin(R_{8n} K_1 X) + Z_6 \cos(R_{8n} K_1 X)\} R_{8n} \quad (\text{eqn A.23})$$

$$P_3 = \sum_{n=1}^{N_1} (-1)^{\text{INT}(N/2)} \{Z_5 \cos(R_{9n} K_1 X) + Z_6 \sin(R_{9n} K_1 X)\} R_{9n} \quad (\text{eqn A.24})$$

$$P_4 = \sum_{n=1}^{N_1} (-1)^{\text{INT}(N/2)} \{-Z_5 \sin(R_{9n} K_1 X) + Z_6 \cos(R_{9n} K_1 X)\} R_{9n} \quad (\text{eqn A.25})$$

$$P_5 = P_1 + P_2 \quad (\text{eqn A.26})$$

$$P_6 = P_3 + P_4 \quad (\text{eqn A.27})$$

$$P_{\text{tot}} = R_1 \sqrt{P_5^2 + P_6^2} \quad (\text{eqn A.28})$$

# APPENDIX B

## DSLOW PROGRAM

```

*****
** THIS PROGRAM CALLED DSLOW IS CALCULATING THE SOUND PRESSURE **
** WITHIN THE WEDGE OVERLYING SLOW BOTTOM FLUID AND DOWN-SLOPE **
** DIRECTION **
*****
-
INTEGER A,I,I1,M,N,S1,S2,N1,J,K,P
REAL*4 B,CC,C2,D,D1,D2,G,PI,P1,P2,Q1,R1,R2,T,
* T4,T6,W0,W1,V0,V1,V2,Z1,Z2,Z3,Z4,Z5,Z6,
* T1(80),R8(80),R9(80),S(30),C(30),E(30),AT(30),
* F(30),V,Z,R3,AL,P2(30),DZ(30),V,DX,XP,DD,PN(30)
-
REAL*4 TQ0,TQ01,TQ02,TQ03
PI=ACOS(-1.0D00)
*****
** INPUT PARAMETERS **
*****
B = WEDGE ANGLE (DEG)
G = SOURCE ANGLE (DEG)
D = RECEIVER ANGLE (DEG)
N1 = # OF IMAGE POINTS
R1 = SOURCE DISTANCE (IN CHARACTERISTIC DISTANCES)
R2 = RECEIVER DISTANCE (IN CHARACTERISTIC DISTANCES)
V0 = APEX DISTANCE (IN CHARACTERISTIC DISTANCES)
D1 =  $\rho_1/\rho_2$ 
CC =  $c_1/c_2$ 
AL = ALPHA/K2
A = # OF RECEIVER POSITIONS
*****
** INITIAL INPUT & RELATIONS **
*****
V0 = 0.00
R2 = 9.00
D0 = 111 P=1.6
B = 10.00
G = 10.00
C2 = 3*B/4
CC = 2*B/4
D1 = 1*B/4
R1 = 0.95
R2 = 1.10
V0 = 1.00
D0 = 0.75
C2 = 1.01
CC = 1.20
D1 = 1.50
R1 = 2.00
R2 = 2.00
V0 = 0.00
D0 = 0.80
CC = 1.10
AL = 0.0001
S = 10
*****
** THE MAIN PROGRAM CALCULATES UPPER AND LOWER PATH OF RAYS **
*****
K = 0
N1 = INT(180./B)
T6 = 180./PI
B = B/T6
G = G/T6
C2 = CC*2
DZ = (V0*V0)+(R1*R1)+(R2*R2)
R3 = 2.*R1*R2
T4 = PI/(2*TAN(ACOS(1/CC))*TAN(B))
TQ0 = TAN(B)
TQ01 = ACOS(1/CC)
TQ02 = TAN(TQ01)
TQ03 = 2.*TQ02*TQ0
T4 = PI/TQ03

```





```

C420 FORMAT(3X,I2,6X,I2,5X,F6.4,10X,F6.4,3X,F6.4,3X,F6.4,10X,F7.4)
C   *WRITE (6,420) N,I2,S(I),T6,E(I),F(I),ATAN(F(I)/E(I))
40 CONTINUE
      Z1 = 0
      Z2 = 0
      Z3 = 0
      Z4 = 0
      Z5 = 0
      Z6 = 0
      IF (N.LE.2.00) GOTO 50
      DO 45 I = 1, I1
        Z1 = S(I)
        Z2 = F(I)
        Z3 = Z1*Z3-Z2*Z4
        Z4 = Z1*Z4+Z2*Z3
      45 CONTINUE
      Z5 = Z5
      Z6 = Z6
      T4 = R8(N)
      C(I) = COS(T4)
      S(I) = SIN(T4)
      Z1 = Z1*Z3-Z2*Z4
      Z2 = Z1*Z4+Z2*Z3
      Z3 = Z3/R8(N)
      Z4 = Z4/R8(N)
C500 FORMAT(6X,N,OF I,P,3X,RE(REFL)=,3X,IM(REFL)=)
C   *WRITE (6,500) N,I2,S(I),T6,E(I),F(I),ATAN(F(I)/E(I))
C510 FORMAT(3X,I2,6X,F6.4,6X,F6.4)
C   *WRITE (6,510) N,I2,S(I),T6,E(I),F(I),ATAN(F(I)/E(I))
C600 *FORMAT(5X,AN2,ARCSIN(S(I))*T6=,3X,E(I),5X,F(I),5X,EF',
C   *WRITE (6,600) I,I1,I1
      DO 60 I = 1, I1
        S(I) = ABS(R1*SIN(T1(N)-2*(I-1)*B)
        *      + R2*SIN(2*(I-1)*B+D))/R9(N)
        C(I) = SORT(1-S(I)*S(I))
        T1 = S(I)/D1
        W0 = -C2+C(I)*C(I)
        W1 = SORT((W0*W0)+(W1*W1))
        Y = ABS(W0)
        IF (Y.LE.Z) Y = Z
        Y1 = 0.1*SORT(Y+W0)
        Y2 = 0.1*SORT(Y-W0)
        T = Y2
        Z1 = -Y1
        Z2 = Z1/(Z1*Z1+Z2*Z2)
        Z3 = -Z2/(Z1*Z1+Z2*Z2)
        Z4 = T+Y2
        Z5 = Z1*Z3-Z2*Z4
        Z6 = Z1*Z4+Z2*Z3
        Z1 = Z5
        Z2 = Z6
        AN1 = ASIN(S(I))*T6
        AN2 = SORT(E(I)*E(I)+F(I)*F(I))
        T6 = ATAN(F(I)/E(I))*T6
C610 FORMAT(2X,I2,5X,F6.4,5X,F6.4,5X,F6.4,5X,F6.4,5X,F7.4)
C   *WRITE (6,610) I,AN1,E(I),F(I),EF,AN2
60 CONTINUE
      Z1 = 0
      Z2 = 0
      Z3 = 0
      Z4 = 0
      Z5 = 0
      Z6 = 0
      DO 80 I = 1, I1
        Z1 = S(I)
        Z2 = F(I)
        Z3 = Z1*Z3-Z2*Z4
        Z4 = Z1*Z4+Z2*Z3
      80 CONTINUE
      Z1 = Z5

```

```

      Z2 = Z6
      T4 = R9(N)
      Z3 = COS(T)
      Z4 = SIN(T)
      Z5 = Z3 - Z2*Z4
      Z6 = Z4 + Z3*Z5
      P1 = P2 + Z5/R9(N)
      P2 = Z6/R9(N)
C700  FORMAT('  LOWER PATH NO= ',3X,'RE(REFL)= ',3X,'IM(REFL)= ')
      WRITE(6,700)
C710  FORMAT(6X,12X,F6.4,12X,F6.4)
      WRITE(6,710) N,S2*Z1,S2*Z2
30  CONTINUE
      K = K+1
      DZ(K) = D*T6
      PZ(K) = SORT(P1*P1+P2*P2)*R1
      AT(K) = ATAN(P2/P1)
      WRITE(6,810) K,DZ(K),PZ(K),ATAN(P2/P1),PN(K)
C810  FORMAT(6X,13,11X,F5.2,12X,F7.4,12X,F7.4,10X,F7.4)
      CONTINUE
C10  CONTINUE
      DO 31 I=1,29
      XP = PZ(28)
      PN(I) = PZ(I)/XP
      WRITE(6,811) I,DZ(I),PZ(I),AT(I),PN(I)
C811  FORMAT(2X,13,7X,F5.2,8X,F9.6,8X,F9.6,6X,F9.6)
      CONTINUE
C31  Y0 = Y0 + 0.5
      Z2 = Z2 + 0.50
C111 CONTINUE
      STOP
      END
*****
** A SUBPROGRAM FOR PLOTTING BY TEK6180R SHERPA **
*****
CALL MEDBUF
CALL TEK618
CALL COMPRES
CALL NOBRDR
CALL PLOTGE(15,12)
CALL PLOTGE(15,9)
CALL HEIGHT(12,9)
CALL XNAME('NORMALIZED PRESSURE AMPLITUDES',29)
CALL YNAME('RECEIVER ANGLE(DEG)',19)
CALL XTICKS(5)
CALL YTIKCS(5)
CALL GRAPT(0,0,10,0,0,0,0,0,0,0,0,0)
CALL GRAPT(0,0,50,0,0,0,0,0,0,0,0,0)
CALL GRAPT(0,0,15,0,0,0,0,0,0,0,0,0)
CALL DOPT
CALL GRID(2,2)
CALL HPRDIN('REC. ANGLE VS. PRESSURES',-100,1.8,1)
CALL MESSAG('WEDGE ANGLE: $ 100 $ ABUT 8.7')
CALL MESSAG('RHO1/RHO2: $ 100 $ ABUT 8.65')
CALL MESSAG('C1/C2: $ 100 $ ABUT 6.0')
CALL MESSAG('SOURCES ANGLE: $ 100 $ ABUT 5.5')
CALL MESSAG('1.2500 $ 100 $ ABUT 5.5')
CALL MESSAG('3.7500 $ 100 $ ABUT 5.5')
CALL MESSAG('7.5000 $ 100 $ ABUT 5.5')
CALL MESSAG('SOURCES DIST: $ 100 $ ABUT 5.5')
CALL MESSAG('1.0000 $ 100 $ ABUT 5.5')
CALL MESSAG('1.6000 $ 100 $ ABUT 5.5')
CALL MESSAG('RECO DIST INIT: $ 100 $ ABUT 4.5')
CALL MESSAG('3.0000 $ 100 $ ABUT 4.5')
CALL MESSAG('3.0000 $ 100 $ ABUT 4.5')
CALL MESSAG('RECO DIST INCRM: $ 100 $ ABUT 4.0')
CALL MESSAG('4.0000 $ 100 $ ABUT 4.0')
CALL MESSAG('SHO DIST INIT: $ 100 $ ABUT 3.5')
CALL MESSAG('1.00 $ 100 $ ABUT 3.5')

```

```

C      CALL MESSAG('SHO.DIST: S',100.8,3.5)
C      CALL MESSAG('O.OO S',100,'ABUT','ABUT')
C      CALL RESULT('ALL')
C      CALL PARC3
C      CALL POLY3
C      CALL NOCHECK
C      CALL CURVE(PN,DZ,29,0)
C111  CONTINUE
C      CALL ENDPL(0)
C      CALL DONEPL
C      STOP
C      END

```

```

*****
** For plotting the calculations result on TEK618 or Sherpa, erase **
** the proper C's in DISPLA subprogram above. Put C's in front of **
** 111 CONTINUE STOP and END in Main Program. **
*****

```

## APPENDIX C

### NUMERICAL RESULTS OF DSLOW

WEDGE ANGLE = 10.00 SOURCE ANGLE = 2.50  
 SOURCE DISTANCE = 0.75 RECEIVER DISTANCE = 9.00 SHORE DISTANCE = 0.00  
 RHO1/RHO2 = 0.80 C1/C2 = 1.10 ALPHA/K2 = 0.0001  
 K1X = 19.44

REC.POS	REC.ANGLE	PRES.AMPLITUDE	PHASE ANGLE	NORM.PRESS
1	0.000	0.000	0.000	0.000
2	0.000	0.000	0.000	0.000
3	0.000	0.000	0.000	0.000
4	0.000	0.000	0.000	0.000
5	0.000	0.000	0.000	0.000
6	0.000	0.000	0.000	0.000
7	0.000	0.000	0.000	0.000
8	0.000	0.000	0.000	0.000
9	0.000	0.000	0.000	0.000
10	0.000	0.000	0.000	0.000
11	0.000	0.000	0.000	0.000
12	0.000	0.000	0.000	0.000
13	0.000	0.000	0.000	0.000
14	0.000	0.000	0.000	0.000
15	0.000	0.000	0.000	0.000
16	0.000	0.000	0.000	0.000
17	0.000	0.000	0.000	0.000
18	0.000	0.000	0.000	0.000
19	0.000	0.000	0.000	0.000
20	0.000	0.000	0.000	0.000
21	0.000	0.000	0.000	0.000
22	0.000	0.000	0.000	0.000
23	0.000	0.000	0.000	0.000
24	0.000	0.000	0.000	0.000
25	0.000	0.000	0.000	0.000
26	0.000	0.000	0.000	0.000
27	0.000	0.000	0.000	0.000
28	0.000	0.000	0.000	0.000
29	0.000	0.000	0.000	0.000
30	0.000	0.000	0.000	0.000
31	0.000	0.000	0.000	0.000
32	0.000	0.000	0.000	0.000
33	0.000	0.000	0.000	0.000
34	0.000	0.000	0.000	0.000
35	0.000	0.000	0.000	0.000
36	0.000	0.000	0.000	0.000
37	0.000	0.000	0.000	0.000
38	0.000	0.000	0.000	0.000
39	0.000	0.000	0.000	0.000
40	0.000	0.000	0.000	0.000
41	0.000	0.000	0.000	0.000
42	0.000	0.000	0.000	0.000
43	0.000	0.000	0.000	0.000
44	0.000	0.000	0.000	0.000
45	0.000	0.000	0.000	0.000
46	0.000	0.000	0.000	0.000
47	0.000	0.000	0.000	0.000
48	0.000	0.000	0.000	0.000
49	0.000	0.000	0.000	0.000
50	0.000	0.000	0.000	0.000
51	0.000	0.000	0.000	0.000
52	0.000	0.000	0.000	0.000
53	0.000	0.000	0.000	0.000
54	0.000	0.000	0.000	0.000
55	0.000	0.000	0.000	0.000
56	0.000	0.000	0.000	0.000
57	0.000	0.000	0.000	0.000
58	0.000	0.000	0.000	0.000
59	0.000	0.000	0.000	0.000
60	0.000	0.000	0.000	0.000
61	0.000	0.000	0.000	0.000
62	0.000	0.000	0.000	0.000
63	0.000	0.000	0.000	0.000
64	0.000	0.000	0.000	0.000
65	0.000	0.000	0.000	0.000
66	0.000	0.000	0.000	0.000
67	0.000	0.000	0.000	0.000
68	0.000	0.000	0.000	0.000
69	0.000	0.000	0.000	0.000
70	0.000	0.000	0.000	0.000
71	0.000	0.000	0.000	0.000
72	0.000	0.000	0.000	0.000
73	0.000	0.000	0.000	0.000
74	0.000	0.000	0.000	0.000
75	0.000	0.000	0.000	0.000
76	0.000	0.000	0.000	0.000
77				

WEDGE ANGLE = 10.00 SOURCE ANGLE = 2.50  
 SOURCE DISTANCE = 0.75 RECEIVER DISTANCE = 4.50 SHORE DISTANCE = 0.00  
 RHO1/RHO2 = 0.80 C1/C2 = 1.10 ALPHA/K2 = 0.0001  
 X1X = 19.44

REC.POS	REC.ANGLE	PRES.AMPLITUDE	PHASE ANGLE	NORM.PRESS
1	0.00	0.00	1.537560	7.554441
2	0.00	0.00	1.537560	7.554441
3	0.00	0.00	1.537560	7.554441
4	0.00	0.00	1.537560	7.554441
5	0.00	0.00	1.537560	7.554441
6	0.00	0.00	1.537560	7.554441
7	0.00	0.00	1.537560	7.554441
8	0.00	0.00	1.537560	7.554441
9	0.00	0.00	1.537560	7.554441
10	0.00	0.00	1.537560	7.554441
11	0.00	0.00	1.537560	7.554441
12	0.00	0.00	1.537560	7.554441
13	0.00	0.00	1.537560	7.554441
14	0.00	0.00	1.537560	7.554441
15	0.00	0.00	1.537560	7.554441
16	0.00	0.00	1.537560	7.554441
17	0.00	0.00	1.537560	7.554441
18	0.00	0.00	1.537560	7.554441
19	0.00	0.00	1.537560	7.554441
20	0.00	0.00	1.537560	7.554441
21	0.00	0.00	1.537560	7.554441
22	0.00	0.00	1.537560	7.554441
23	0.00	0.00	1.537560	7.554441
24	0.00	0.00	1.537560	7.554441
25	0.00	0.00	1.537560	7.554441
26	0.00	0.00	1.537560	7.554441
27	0.00	0.00	1.537560	7.554441
28	0.00	0.00	1.537560	7.554441
29	0.00	0.00	1.537560	7.554441
30	0.00	0.00	1.537560	7.554441
31	0.00	0.00	1.537560	7.554441
32	0.00	0.00	1.537560	7.554441
33	0.00	0.00	1.537560	7.554441
34	0.00	0.00	1.537560	7.554441
35	0.00	0.00	1.537560	7.554441
36	0.00	0.00	1.537560	7.554441
37	0.00	0.00	1.537560	7.554441
38	0.00	0.00	1.537560	7.554441
39	0.00	0.00	1.537560	7.554441
40	0.00	0.00	1.537560	7.554441
41	0.00	0.00	1.537560	7.554441
42	0.00	0.00	1.537560	7.554441
43	0.00	0.00	1.537560	7.554441
44	0.00	0.00	1.537560	7.554441
45	0.00	0.00	1.537560	7.554441
46	0.00	0.00	1.537560	7.554441
47	0.00	0.00	1.537560	7.554441
48	0.00	0.00	1.537560	7.554441
49	0.00	0.00	1.537560	7.554441
50	0.00	0.00	1.537560	7.554441
51	0.00	0.00	1.537560	7.554441
52	0.00	0.00	1.537560	7.554441
53	0.00	0.00	1.537560	7.554441
54	0.00	0.00	1.537560	7.554441
55	0.00	0.00	1.537560	7.554441
56	0.00	0.00	1.537560	7.554441
57	0.00	0.00	1.537560	7.554441
58	0.00	0.00	1.537560	7.554441
59	0.00	0.00	1.537560	7.554441
60	0.00	0.00	1.537560	7.554441
61	0.00	0.00	1.537560	7.554441
62	0.00	0.00	1.537560	7.554441
63	0.00	0.00	1.537560	7.554441
64	0.00	0.00	1.537560	7.554441
65	0.00	0.00	1.537560	7.554441
66	0.00	0.00	1.537560	7.554441
67	0.00	0.00	1.537560	7.554441
68	0.00	0.00	1.537560	7.554441
69	0.00	0.00	1.537560	7.554441
70	0.00	0.00	1.537560	7.554441
71	0.00	0.00	1.537560	7.554441
72	0.00	0.00	1.537560	7.554441
73	0.00	0.00	1.537560	7.554441
74	0.00	0.00	1.537560	7.554441
75	0.00	0.00	1.537560	7.554441
76	0.00	0.00	1.537560	7.554441
77	0.00	0.00	1.537560	7.554441
78	0.00	0.00	1.537560	7.554441
79	0.00	0.00	1.537560	7.554441
80	0.00	0.00	1.537560	7.554441
81	0.00	0.00	1.537560	7.554441
82	0.00	0.00	1.537560	7.554441
83	0.00	0.00	1.537560	7.554441
84	0.00	0.00	1.537560	7.554441
85	0.00	0.00	1.537560	7.554441
86	0.00	0.00	1.537560	7.554441
87	0.00	0.00	1.537560	7.554441
88	0.00	0.00	1.537560	7.554441
89	0.00	0.00	1.537560	7.554441
90	0.00	0.00	1.537560	7.554441
91	0.00	0.00	1.537560	7.554441
92	0.00	0.00	1.537560	7.554441
93	0.00	0.00	1.537560	7.554441
94	0.00	0.00	1.537560	7.554441
95	0.00	0.00	1.537560	7.554441
96	0.00	0.00	1.537560	7.554441
97	0.00	0.00	1.537560	7.554441
98	0.00	0.00	1.537560	7.554441
99	0.00	0.00	1.537560	7.554441
100	0.00	0.00	1.537560	7.554441

WEDGE ANGLE = 10.00 SOURCE ANGLE = 2.50  
 SOURCE DISTANCE = 0.75 RECEIVER DISTANCE = 2.25 SHORE DISTANCE = 0.00  
 RHO1/RHO2 = 0.80 C1/C2 = 1.10 ALPHA/K2 = 0.0001  
 K1X = 19.44

REC.POS	REC.ANGLE	PRES.AMPLITUDE	PHASE ANGLE	NORM.PRESS
1	0	0.2244816	1.0084841	6.519929
2	0	0.2244816	1.0084841	6.519929
3	0	0.2244816	1.0084841	6.519929
4	0	0.2244816	1.0084841	6.519929
5	0	0.2244816	1.0084841	6.519929
6	0	0.2244816	1.0084841	6.519929
7	0	0.2244816	1.0084841	6.519929
8	0	0.2244816	1.0084841	6.519929
9	0	0.2244816	1.0084841	6.519929
10	0	0.2244816	1.0084841	6.519929
11	0	0.2244816	1.0084841	6.519929
12	0	0.2244816	1.0084841	6.519929
13	0	0.2244816	1.0084841	6.519929
14	0	0.2244816	1.0084841	6.519929
15	0	0.2244816	1.0084841	6.519929
16	0	0.2244816	1.0084841	6.519929
17	0	0.2244816	1.0084841	6.519929
18	0	0.2244816	1.0084841	6.519929
19	0	0.2244816	1.0084841	6.519929
20	0	0.2244816	1.0084841	6.519929
21	0	0.2244816	1.0084841	6.519929
22	0	0.2244816	1.0084841	6.519929
23	0	0.2244816	1.0084841	6.519929
24	0	0.2244816	1.0084841	6.519929
25	0	0.2244816	1.0084841	6.519929
26	0	0.2244816	1.0084841	6.519929
27	0	0.2244816	1.0084841	6.519929
28	0	0.2244816	1.0084841	6.519929
29	0	0.2244816	1.0084841	6.519929
30	0	0.2244816	1.0084841	6.519929
31	0	0.2244816	1.0084841	6.519929
32	0	0.2244816	1.0084841	6.519929
33	0	0.2244816	1.0084841	6.519929
34	0	0.2244816	1.0084841	6.519929
35	0	0.2244816	1.0084841	6.519929
36	0	0.2244816	1.0084841	6.519929
37	0	0.2244816	1.0084841	6.519929
38	0	0.2244816	1.0084841	6.519929
39	0	0.2244816	1.0084841	6.519929
40	0	0.2244816	1.0084841	6.519929
41	0	0.2244816	1.0084841	6.519929
42	0	0.2244816	1.0084841	6.519929
43	0	0.2244816	1.0084841	6.519929
44	0	0.2244816	1.0084841	6.519929
45	0	0.2244816	1.0084841	6.519929
46	0	0.2244816	1.0084841	6.519929
47	0	0.2244816	1.0084841	6.519929
48	0	0.2244816	1.0084841	6.519929
49	0	0.2244816	1.0084841	6.519929
50	0	0.2244816	1.0084841	6.519929
51	0	0.2244816	1.0084841	6.519929
52	0	0.2244816	1.0084841	6.519929
53	0	0.2244816	1.0084841	6.519929
54	0	0.2244816	1.0084841	6.519929
55	0	0.2244816	1.0084841	6.519929
56	0	0.2244816	1.0084841	6.519929
57	0	0.2244816	1.0084841	6.519929
58	0	0.2244816	1.0084841	6.519929
59	0	0.2244816	1.0084841	6.519929
60	0	0.2244816	1.0084841	6.519929
61	0	0.2244816	1.0084841	6.519929
62	0	0.2244816	1.0084841	6.519929
63	0	0.2244816	1.0084841	6.519929
64	0	0.2244816	1.0084841	6.519929
65	0	0.2244816	1.0084841	6.519929
66	0	0.2244816	1.0084841	6.519929
67	0	0.2244816	1.0084841	6.519929
68	0	0.2244816	1.0084841	6.519929
69	0	0.2244816	1.0084841	6.519929
70	0	0.2244816	1.0084841	6.519929
71	0	0.2244816	1.0084841	6.519929
72	0	0.2244816	1.0084841	6.519929
73	0	0.2244816	1.0084841	6.519929
74	0	0.2244816	1.0084841	6.519929
75	0	0.2244816	1.0084841	6.519929
76	0	0.2244816	1.0084841	6.519929
77	0	0.2244816	1.0084841	6.519929
78	0	0.2244816	1.0084841	6.519929
79	0	0.2244816	1.0084841	6.519929
80	0	0.2244816	1.0084841	6.519929
81	0	0.2244816	1.0084841	6.519929
82	0	0.2244816	1.0084841	6.519929
83	0	0.2244816	1.0084841	6.519929
84	0	0.2244816	1.0084841	6.519929
85	0	0.2244816	1.0084841	6.519929
86	0	0.2244816	1.0084841	6.519929
87	0	0.2244816	1.0084841	6.519929
88	0	0.2244816	1.0084841	6.519929
89	0	0.2244816	1.0084841	6.519929
90	0	0.2244816	1.0084841	6.519929
91	0	0.2244816	1.0084841	6.519929
92	0	0.2244816	1.0084841	6.519929
93	0	0.2244816	1.0084841	6.519929
94	0	0.2244816	1.0084841	6.519929
95	0	0.2244816	1.0084841	6.519929
96	0	0.2244816	1.0084841	6.519929
97	0	0.2244816	1.0084841	6.519929
98	0	0.2244816	1.0084841	6.519929
99	0	0.2244816	1.0084841	6.519929
100	0	0.2244816	1.0084841	6.519929

WEDGE ANGLE = 10.00 SOURCE ANGLE = 2.50  
 SOURCE DISTANCE = 0.75 RECEIVER DISTANCE = 1.13 SHORE DISTANCE = 0.00  
 RHO1/RHO2 = 0.80 C1/C2 = 1.10 ALPHA/K2 = 0.0001  
 K1X = 19.44

REC.POS	REC.ANGLE	PRES.AMPLITUDE	PHASE ANGLE	NORM.PRESS
1	00	1	-0	4
2	00	1	00	7
3	00	1	00	4
4	00	1	00	4
5	00	1	00	4
6	00	1	00	4
7	00	1	00	4
8	00	1	00	4
9	00	1	00	4
10	00	1	00	4
11	00	1	00	4
12	00	1	00	4
13	00	1	00	4
14	00	1	00	4
15	00	1	00	4
16	00	1	00	4
17	00	1	00	4
18	00	1	00	4
19	00	1	00	4
20	00	1	00	4
21	00	1	00	4
22	00	1	00	4
23	00	1	00	4
24	00	1	00	4
25	00	1	00	4
26	00	1	00	4
27	00	1	00	4
28	00	1	00	4
29	00	1	00	4
30	00	1	00	4
31	00	1	00	4
32	00	1	00	4
33	00	1	00	4
34	00	1	00	4
35	00	1	00	4
36	00	1	00	4
37	00	1	00	4
38	00	1	00	4
39	00	1	00	4
40	00	1	00	4
41	00	1	00	4
42	00	1	00	4
43	00	1	00	4
44	00	1	00	4
45	00	1	00	4
46	00	1	00	4
47	00	1	00	4
48	00	1	00	4
49	00	1	00	4
50	00	1	00	4
51	00	1	00	4
52	00	1	00	4
53	00	1	00	4
54	00	1	00	4
55	00	1	00	4
56	00	1	00	4
57	00	1	00	4
58	00	1	00	4
59	00	1	00	4
60	00	1	00	4
61	00	1	00	4
62	00	1	00	4
63	00	1	00	4
64	00	1	00	4
65	00	1	00	4
66	00	1	00	4
67	00	1	00	4
68	00	1	00	4
69	00	1	00	4
70	00	1	00	4
71	00	1	00	4
72	00	1	00	4
73	00	1	00	4
74	00	1	00	4
75	00	1	00	4
76	00	1	00	4
77	00	1	00	4
78	00	1	00	4
79	00	1	00	4
80	00	1	00	4
81	00	1	00	4
82	00	1	00	4
83	00	1	00	4
84	00	1	00	4
85	00	1	00	4
86	00	1	00	4
87	00	1	00	4
88	00	1	00	4
89	00	1	00	4
90	00	1	00	4
91	00	1	00	4
92	00	1	00	4
93	00	1	00	4
94	00	1	00	4
95	00	1	00	4
96	00	1	00	4
97	00	1	00	4
98	00	1	00	4
99	00	1	00	4
100	00	1	00	4

WEDGE ANGLE = 10.00 SOURCE ANGLE = 2.50  
 SOURCE DISTANCE = 0.75 RECEIVER DISTANCE = 0.56 SHORE DISTANCE = 0.00  
 RHO1/RHO2 = 0.80 C1/C2 = 1.10 ALPHA/K2 = 0.0001  
 K1X = 19.44

REC.POS	REC.ANGLE	PRES.AMPLITUDE	PHASE ANGLE	NORM.PRESS
1	0.00	3.00	0.00	5.00
2	0.00	3.00	0.00	5.00
3	0.00	3.00	0.00	5.00
4	0.00	3.00	0.00	5.00
5	0.00	3.00	0.00	5.00
6	0.00	3.00	0.00	5.00
7	0.00	3.00	0.00	5.00
8	0.00	3.00	0.00	5.00
9	0.00	3.00	0.00	5.00
10	0.00	3.00	0.00	5.00
11	0.00	3.00	0.00	5.00
12	0.00	3.00	0.00	5.00
13	0.00	3.00	0.00	5.00
14	0.00	3.00	0.00	5.00
15	0.00	3.00	0.00	5.00
16	0.00	3.00	0.00	5.00
17	0.00	3.00	0.00	5.00
18	0.00	3.00	0.00	5.00
19	0.00	3.00	0.00	5.00
20	0.00	3.00	0.00	5.00
21	0.00	3.00	0.00	5.00
22	0.00	3.00	0.00	5.00
23	0.00	3.00	0.00	5.00
24	0.00	3.00	0.00	5.00
25	0.00	3.00	0.00	5.00
26	0.00	3.00	0.00	5.00
27	0.00	3.00	0.00	5.00
28	0.00	3.00	0.00	5.00
29	0.00	3.00	0.00	5.00
30	0.00	3.00	0.00	5.00
31	0.00	3.00	0.00	5.00
32	0.00	3.00	0.00	5.00
33	0.00	3.00	0.00	5.00
34	0.00	3.00	0.00	5.00
35	0.00	3.00	0.00	5.00
36	0.00	3.00	0.00	5.00
37	0.00	3.00	0.00	5.00
38	0.00	3.00	0.00	5.00
39	0.00	3.00	0.00	5.00
40	0.00	3.00	0.00	5.00
41	0.00	3.00	0.00	5.00
42	0.00	3.00	0.00	5.00
43	0.00	3.00	0.00	5.00
44	0.00	3.00	0.00	5.00
45	0.00	3.00	0.00	5.00
46	0.00	3.00	0.00	5.00
47	0.00	3.00	0.00	5.00
48	0.00	3.00	0.00	5.00
49	0.00	3.00	0.00	5.00
50	0.00	3.00	0.00	5.00
51	0.00	3.00	0.00	5.00
52	0.00	3.00	0.00	5.00
53	0.00	3.00	0.00	5.00
54	0.00	3.00	0.00	5.00
55	0.00	3.00	0.00	5.00
56	0.00	3.00	0.00	5.00
57	0.00	3.00	0.00	5.00
58	0.00	3.00	0.00	5.00
59	0.00	3.00	0.00	5.00
60	0.00	3.00	0.00	5.00
61	0.00	3.00	0.00	5.00
62	0.00	3.00	0.00	5.00
63	0.00	3.00	0.00	5.00
64	0.00	3.00	0.00	5.00
65	0.00	3.00	0.00	5.00
66	0.00	3.00	0.00	5.00
67	0.00	3.00	0.00	5.00
68	0.00	3.00	0.00	5.00
69	0.00	3.00	0.00	5.00
70	0.00	3.00	0.00	5.00
71	0.00	3.00	0.00	5.00
72	0.00	3.00	0.00	5.00
73	0.00	3.00	0.00	5.00
74	0.00	3.00	0.00	5.00
75	0.00	3.00	0.00	5.00
76	0.00	3.00	0.00	5.00
77	0.00	3.00	0.00	5.00
78	0.00	3.00	0.00	5.00
79	0.00	3.00	0.00	5.00
80	0.00	3.00	0.00	5.00
81	0.00	3.00	0.00	5.00
82	0.00	3.00	0.00	5.00
83	0.00	3.00	0.00	5.00
84	0.00	3.00	0.00	5.00
85	0.00	3.00	0.00	5.00
86	0.00	3.00	0.00	5.00
87	0.00	3.00	0.00	5.00
88	0.00	3.00	0.00	5.00
89	0.00	3.00	0.00	5.00
90	0.00	3.00	0.00	5.00
91	0.00	3.00	0.00	5.00
92	0.00	3.00	0.00	5.00
93	0.00	3.00	0.00	5.00
94	0.00	3.00	0.00	5.00
95	0.00	3.00	0.00	5.00
96	0.00	3.00	0.00	5.00
97	0.00	3.00	0.00	5.00
98	0.00	3.00	0.00	5.00
99	0.00	3.00	0.00	5.00
100	0.00	3.00	0.00	5.00



WEDGE ANGLE = 10.00 SOURCE ANGLE = 2.50  
 SOURCE DISTANCE = 0.75 RECEIVER DISTANCE = 0.28 SHORE DISTANCE = 0.00  
 RHO1/RHO2 = 0.80 C1/C2 = 1.10 ALPHA/K2 = 0.0001  
 K1X = 19.44

REC.POS	REC.ANGLE	PRES.AMPLITUDE	PHASE ANGLE	NORM.PRESS
1	0.00	0.64	0.27	0.00
2	0.00	0.64	0.27	0.00
3	0.00	0.64	0.27	0.00
4	0.00	0.64	0.27	0.00
5	0.00	0.64	0.27	0.00
6	0.00	0.64	0.27	0.00
7	0.00	0.64	0.27	0.00
8	0.00	0.64	0.27	0.00
9	0.00	0.64	0.27	0.00
10	0.00	0.64	0.27	0.00
11	0.00	0.64	0.27	0.00
12	0.00	0.64	0.27	0.00
13	0.00	0.64	0.27	0.00
14	0.00	0.64	0.27	0.00
15	0.00	0.64	0.27	0.00
16	0.00	0.64	0.27	0.00
17	0.00	0.64	0.27	0.00
18	0.00	0.64	0.27	0.00
19	0.00	0.64	0.27	0.00
20	0.00	0.64	0.27	0.00
21	0.00	0.64	0.27	0.00
22	0.00	0.64	0.27	0.00
23	0.00	0.64	0.27	0.00
24	0.00	0.64	0.27	0.00
25	0.00	0.64	0.27	0.00
26	0.00	0.64	0.27	0.00
27	0.00	0.64	0.27	0.00
28	0.00	0.64	0.27	0.00
29	0.00	0.64	0.27	0.00
30	0.00	0.64	0.27	0.00
31	0.00	0.64	0.27	0.00
32	0.00	0.64	0.27	0.00
33	0.00	0.64	0.27	0.00
34	0.00	0.64	0.27	0.00
35	0.00	0.64	0.27	0.00
36	0.00	0.64	0.27	0.00
37	0.00	0.64	0.27	0.00
38	0.00	0.64	0.27	0.00
39	0.00	0.64	0.27	0.00
40	0.00	0.64	0.27	0.00
41	0.00	0.64	0.27	0.00
42	0.00	0.64	0.27	0.00
43	0.00	0.64	0.27	0.00
44	0.00	0.64	0.27	0.00
45	0.00	0.64	0.27	0.00
46	0.00	0.64	0.27	0.00
47	0.00	0.64	0.27	0.00
48	0.00	0.64	0.27	0.00
49	0.00	0.64	0.27	0.00
50	0.00	0.64	0.27	0.00
51	0.00	0.64	0.27	0.00
52	0.00	0.64	0.27	0.00
53	0.00	0.64	0.27	0.00
54	0.00	0.64	0.27	0.00
55	0.00	0.64	0.27	0.00
56	0.00	0.64	0.27	0.00
57	0.00	0.64	0.27	0.00
58	0.00	0.64	0.27	0.00
59	0.00	0.64	0.27	0.00
60	0.00	0.64	0.27	0.00
61	0.00	0.64	0.27	0.00
62	0.00	0.64	0.27	0.00
63	0.00	0.64	0.27	0.00
64	0.00	0.64	0.27	0.00
65	0.00	0.64	0.27	0.00
66	0.00	0.64	0.27	0.00
67	0.00	0.64	0.27	0.00
68	0.00	0.64	0.27	0.00
69	0.00	0.64	0.27	0.00
70	0.00	0.64	0.27	0.00
71	0.00	0.64	0.27	0.00
72	0.00	0.64	0.27	0.00
73	0.00	0.64	0.27	0.00
74	0.00	0.64	0.27	0.00
75	0.00	0.64	0.27	0.00
76	0.00	0.64	0.27	0.00
77	0.00	0.64	0.27	0.00
78	0.00	0.64	0.27	0.00
79	0.00	0.64	0.27	0.00
80	0.00	0.64	0.27	0.00
81	0.00	0.64	0.27	0.00
82	0.00	0.64	0.27	0.00
83	0.00	0.64	0.27	0.00
84	0.00	0.64	0.27	0.00
85	0.00	0.64	0.27	0.00
86	0.00	0.64	0.27	0.00
87	0.00	0.64	0.27	0.00
88	0.00	0.64	0.27	0.00
89	0.00	0.64	0.27	0.00
90	0.00	0.64	0.27	0.00
91	0.00	0.64	0.27	0.00
92	0.00	0.64	0.27	0.00
93	0.00	0.64	0.27	0.00
94	0.00	0.64	0.27	0.00
95	0.00	0.64	0.27	0.00
96	0.00	0.64	0.27	0.00
97	0.00	0.64	0.27	0.00
98	0.00	0.64	0.27	0.00
99	0.00	0.64	0.27	0.00
100	0.00	0.64	0.27	0.00

# **APPENDIX D** **TABLES**

TABLE 1  
RECEIVER DISTANCE AT THE FIRST TRANSITION POINT,  
FOR CONSTANT  $\rho_1 \rho_2 = 0.80$ ,  $c_1 c_2 = 1.10$

$\beta = 6^\circ$ ,  $K_1 X = 32.61$

	$R_1 = 1.10$	$R_1 = 1.20$	$R_1 = 1.30$	$R_1 = 1.40$	$R_1 = 1.50$
$\gamma = \beta/4$	5.2	5.0	5.9	7.3	9.8
$\gamma = \beta/2$	5.2	4.7	5.7	6.8	9.9
$\gamma = 3\beta/4$	4.0	4.5	5.4	7.0	10.5

$\beta = 10^\circ$ ,  $K_1 X = 19.44$

	$R_1 = 0.80$	$R_1 = 0.90$	$R_1 = 1.00$	$R_1 = 1.10$	$R_1 = 1.20$
$\gamma = \beta/4$	17.5	24.0	33.0	52.0	72.0
$\gamma = \beta/2$	12.5	17.0	24.0	42.0	60.0
$\gamma = 3\beta/4$	10.6	17.0	22.0	40.0	58.0

$\beta = 15^\circ$ ,  $K_1 X = 12.79$

	$R_1 = 1.30$	$R_1 = 1.40$	$R_1 = 1.50$	$R_1 = 1.60$	$R_1 = 1.70$
$\gamma = \beta/4$	8.1	8.2	8.7	9.8	11.4
$\gamma = \beta/2$	6.9	7.0	7.8	8.9	10.9
$\gamma = 3\beta/4$	9.8	12.0	15.0	19.0	29.0

TABLE 2  
RECEIVER DISTANCE AT THE FIRST TRANSITION POINT,  
FOR CONSTANT  $\rho_1$   $\rho_2 = 0.80$ ,  $c_1$   $c_2 = 1.20$

$\beta = 6^\circ$ ,  $K_1 X = 22.53$

	$R_1 = 1.30$	$R_1 = 1.40$	$R_1 = 1.50$	$R_1 = 1.60$	$R_1 = 1.70$
$\gamma = \beta/4$	3.37	3.6	3.92	4.4	4.96
$\gamma = \beta/2$	3.155	3.42	3.78	4.36	4.96
$\gamma = 3\beta/4$	3.07	3.34	3.74	4.2	5.1

$\beta = 10^\circ$ ,  $K_1 X = 13.43$

	$R_1 = 0.80$	$R_1 = 0.90$	$R_1 = 1.00$	$R_1 = 1.10$	$R_1 = 1.20$
$\gamma = \beta/4$	6.1	11.3	18.0	40.0	60.0
$\gamma = \beta/2$	6.5	8.2	14.5	25.0	40.0
$\gamma = 3\beta/4$	5.05	5.45	12.0	18.0	30.0

$\beta = 15^\circ$ ,  $K_1 X = 8.84$

	$R_1 = 0.80$	$R_1 = 0.90$	$R_1 = 1.00$	$R_1 = 1.10$	$R_1 = 1.20$
$\gamma = \beta/4$	36.0	40.0	52.0	60.0	64.0
$\gamma = \beta/2$	24.0	26.0	32.0	46.0	54.0
$\gamma = 3\beta/4$	19.50	23.0	28.0	38.0	58.0

TABLE 3  
RECEIVER DISTANCE AT THE FIRST TRANSITION POINT,  
FOR CONSTANT  $\rho_1$   $\rho_2 = 0.90$ ,  $c_1$   $c_2 = 1.10$

$\beta = 6^\circ$ ,  $K_1 X = 32.61$

	$R_1 = 1.10$	$R_1 = 1.20$	$R_1 = 1.30$	$R_1 = 1.40$	$R_1 = 1.50$
$\gamma = \beta/4$	3.66	4.1	4.9	6.2	11.0
$\gamma = \beta/2$	3.35	3.9	4.7	7.0	no
$\gamma = 3\beta/4$	3.24	3.76	4.75	7.3	9.8

$\beta = 10^\circ$ ,  $K_1 X = 19.44$

	$R_1 = 1.30$	$R_1 = 1.40$	$R_1 = 1.50$	$R_1 = 1.60$	$R_1 = 1.70$
$\gamma = \beta/4$	9.8	11.0	14.0	40.0	60.0
$\gamma = \beta/2$	7.6	8.6	11.0	19.0	40.0
$\gamma = 3\beta/4$	6.7	7.6	10.0	21.0	45.0

# APPENDIX E GRAPHS OF $R_1$ VERSUS $R_2$ AT THE FIRST TRANSITION POINT

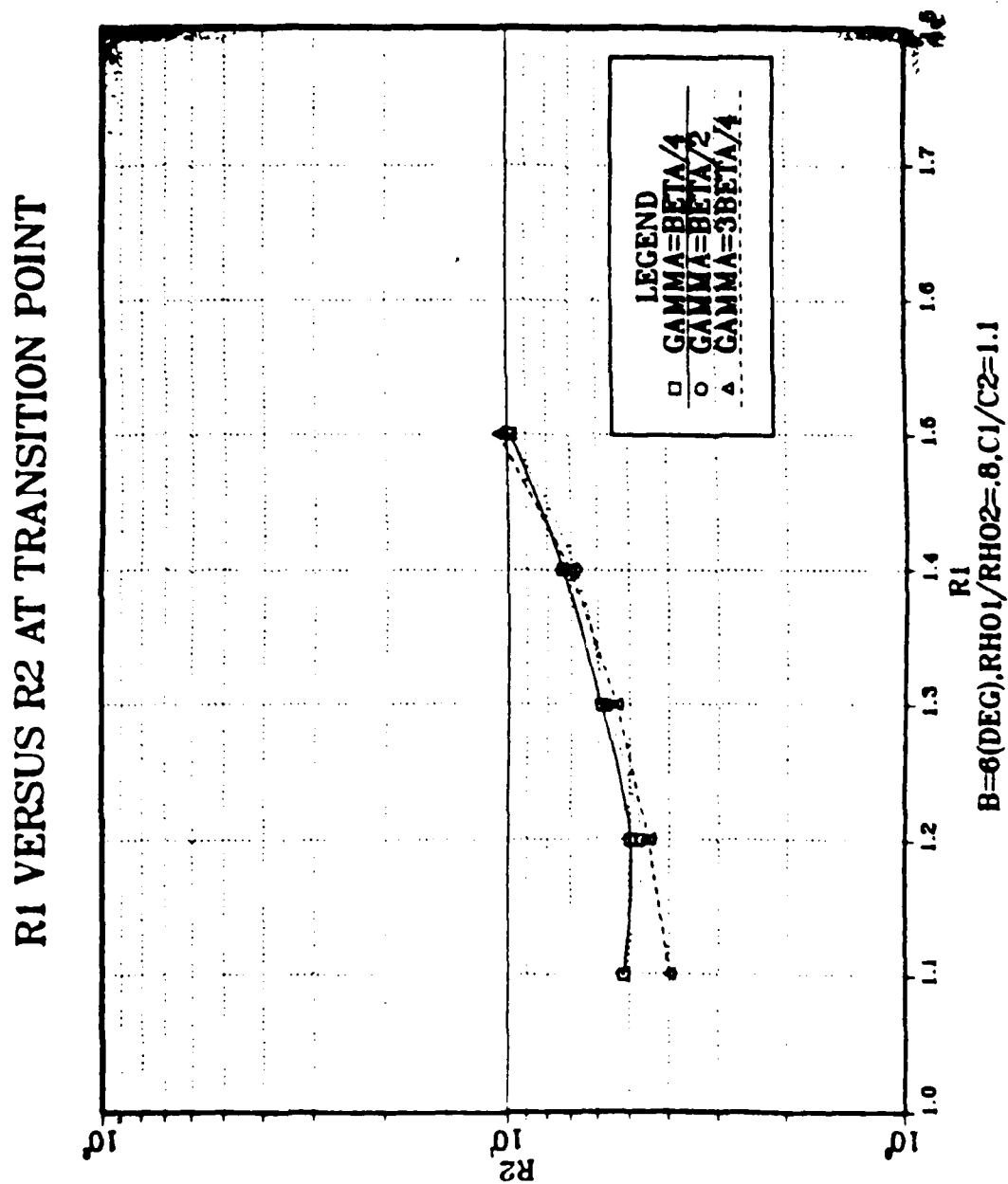


Figure E.1  $R_1$  vs  $R_2$  at the first trans.points, for  $\beta = 6^\circ$ ,  $\rho_1/\rho_2 = 0.80$ ,  $c_1/c_2 = 1.10$ .

# R1 VERSUS R2 AT TRANSITION POINT

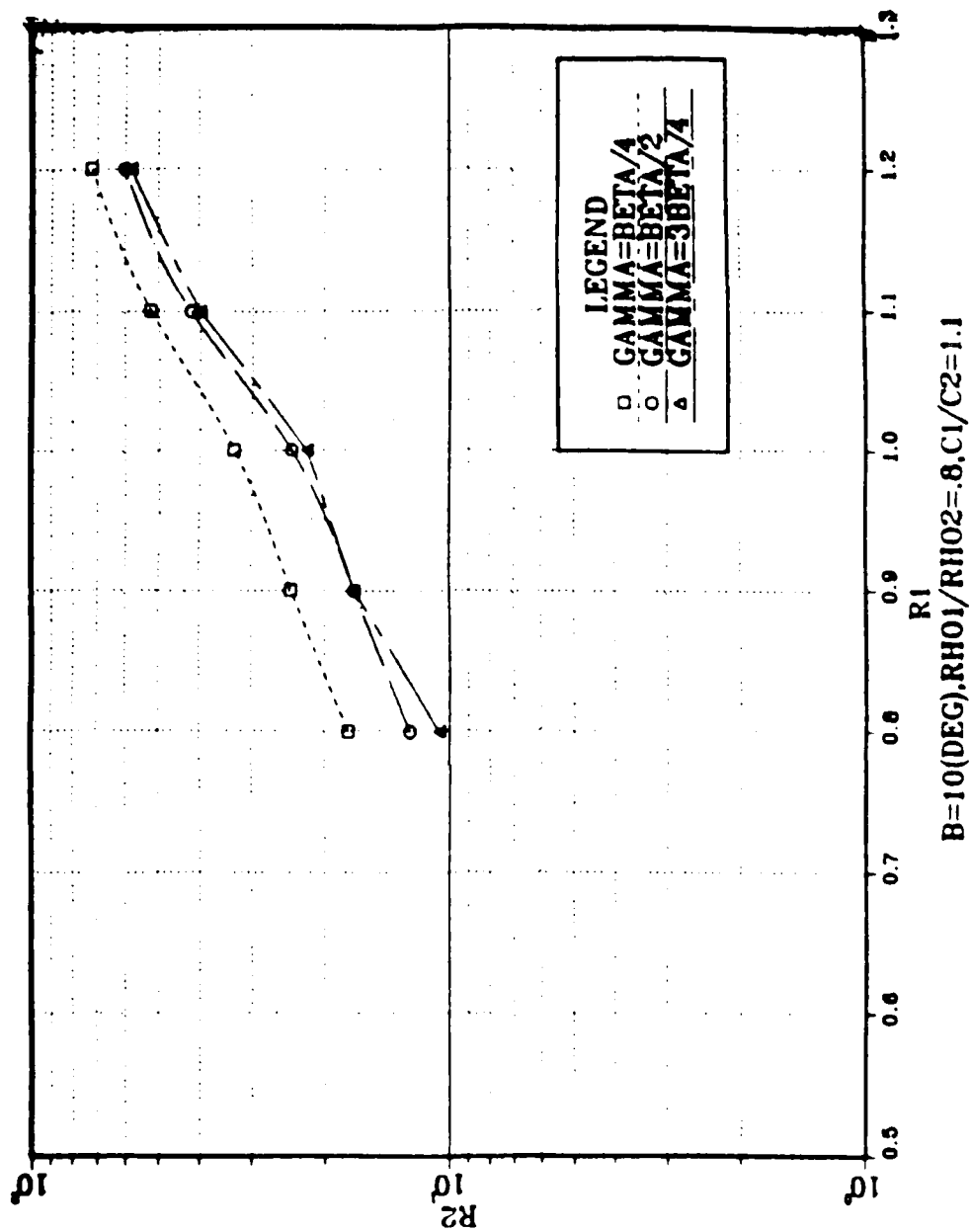


Figure E.2  $R_1$  vs  $R_2$  at the first trans. points, for  $\beta = 10^\circ$ ,  $\rho_1 \rho_2 = 0.80$ ,  $c_1 c_2 = 1.10$ .

# R<sub>1</sub> VERSUS R<sub>2</sub> AT TRANSITION POINT

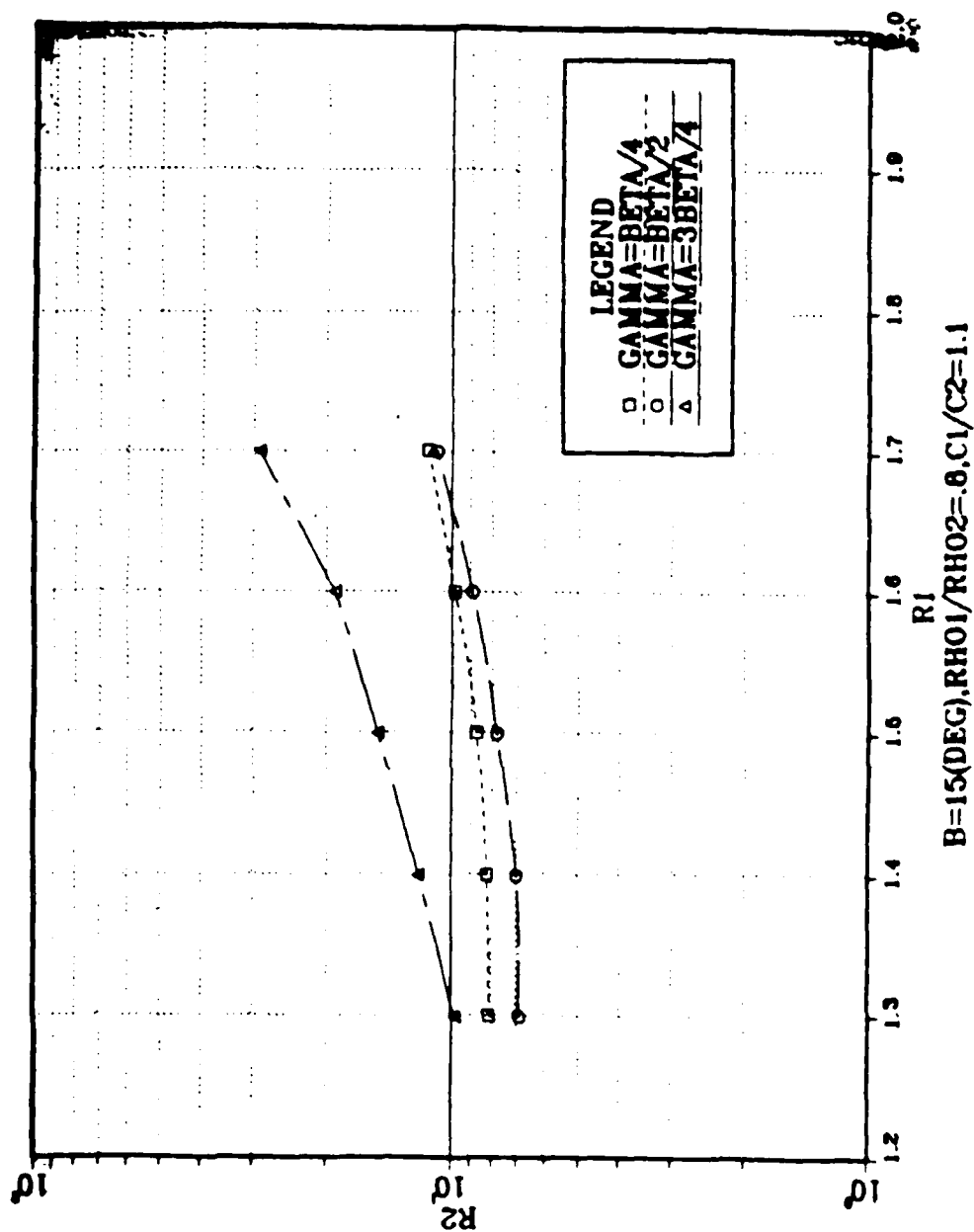


Figure E.3 R<sub>1</sub> vs R<sub>2</sub> at the first trans. points, for  $\beta = 15^\circ$ ,  $\rho_1/\rho_2 = 0.80$ ,  $c_1/c_2 = 1.10$ .

# R<sub>1</sub> VERSUS R<sub>2</sub> AT TRANSITION POINT

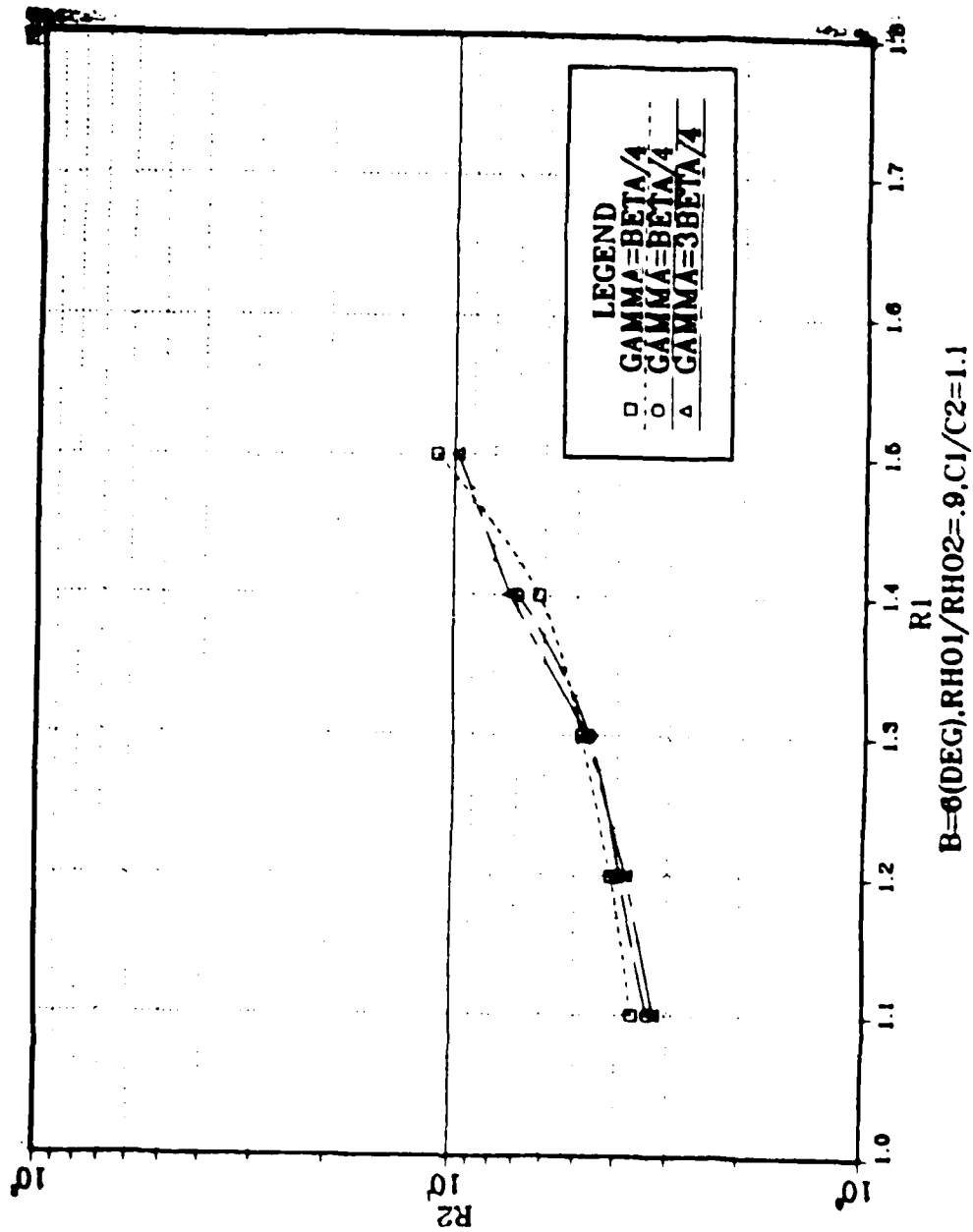


Figure E.4 R<sub>1</sub> vs R<sub>2</sub> at the first trans. points, for  $\beta = 6^\circ$ ,  $\rho_1/\rho_2 = 0.80$ ,  $c_1/c_2 = 1.20$ .



# R<sub>1</sub> VERSUS R<sub>2</sub> AT TRANSITION POINT

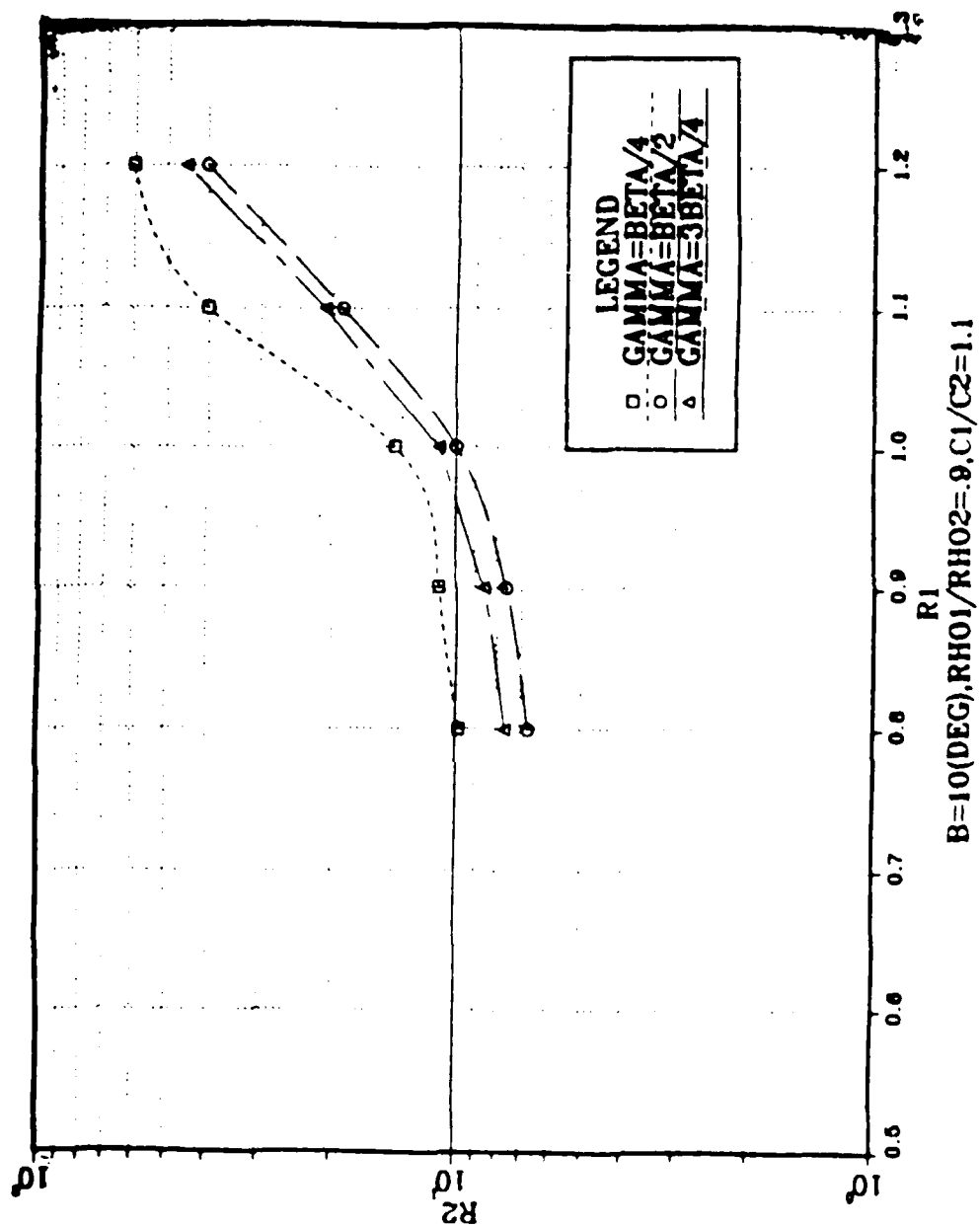


Figure E.5  $R_1$  vs  $R_2$  at the first trans. points, for  $\beta = 10^\circ$ ,  $\rho_1/\rho_2 = 0.80$ ,  $c_1/c_2 = 1.20$ .

# R<sub>1</sub> VERSUS R<sub>2</sub> AT TRANSITION POINT

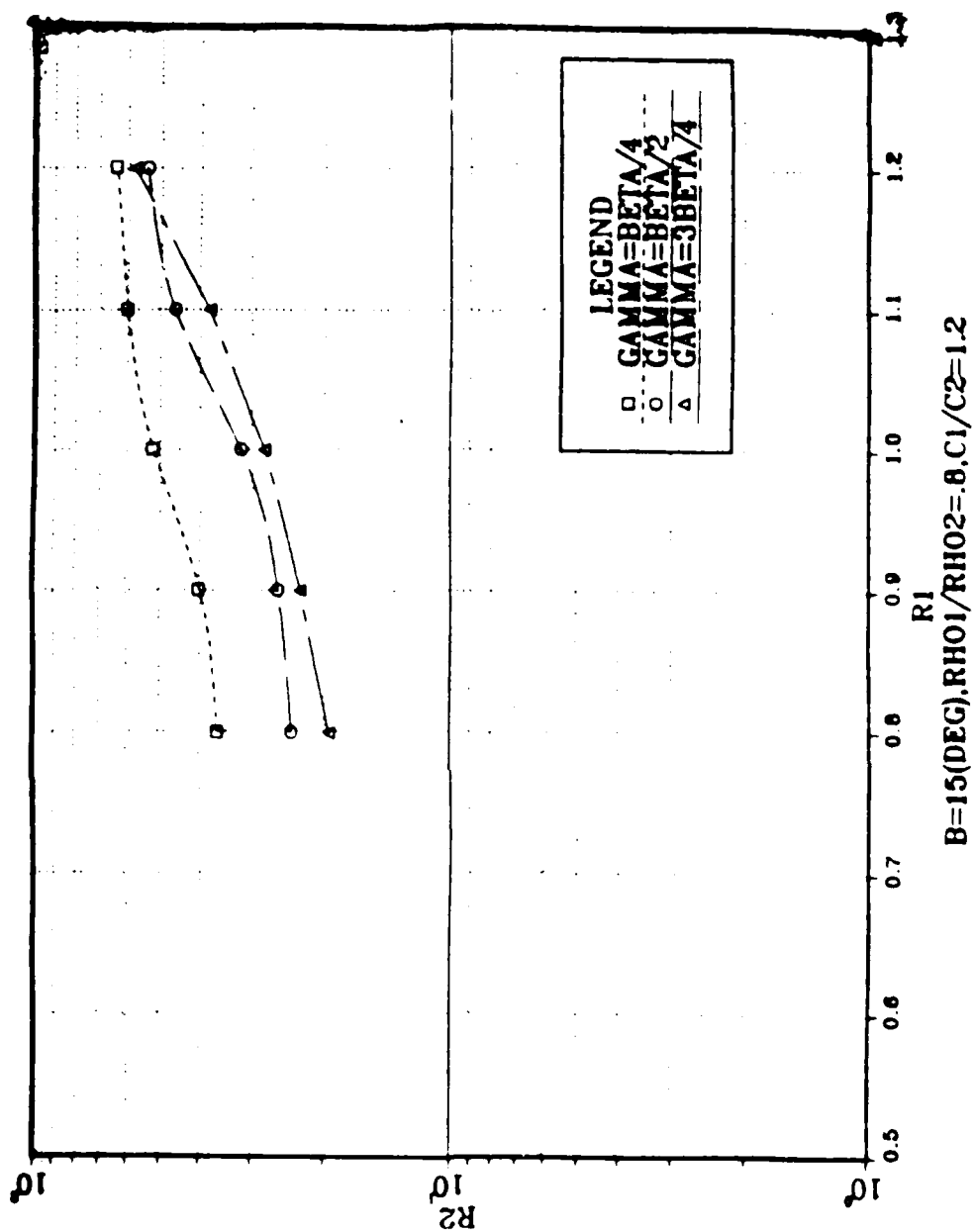


Figure E.6  $R_1$  vs  $R_2$  at the first trans. points, for  $\beta = 15^\circ$ ,  $\rho_1/\rho_2 = 0.80$ ,  $c_1/c_2 = 1.20$ .

# R<sub>1</sub> VERSUS R<sub>2</sub> AT TRANSITION POINT

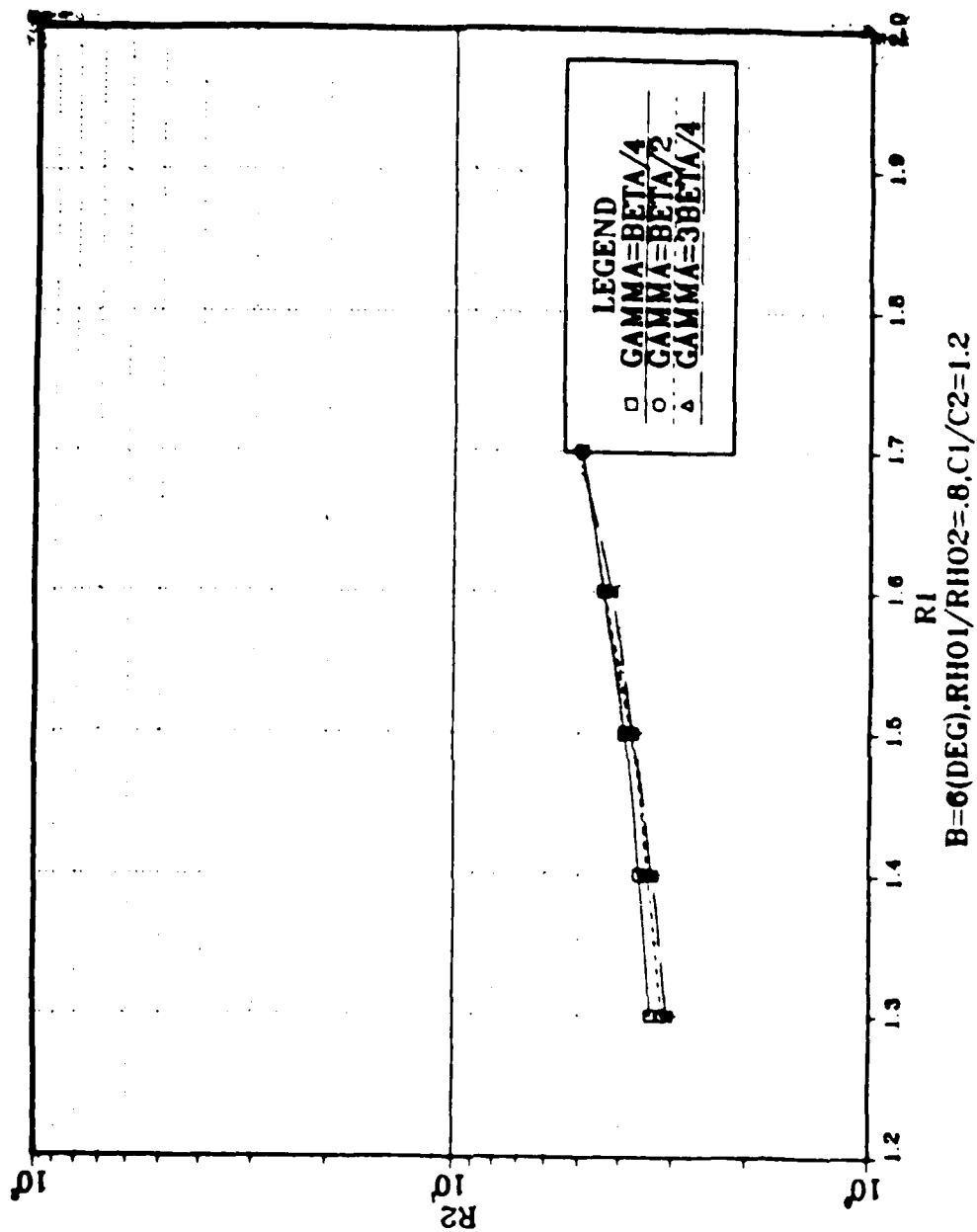


Figure E.7 R<sub>1</sub> vs R<sub>2</sub> at the first trans. points, for  $\beta = 6^\circ$ ,  $\rho_1/\rho_2 = 0.90$ ,  $c_1/c_2 = 1.10$ .

# R<sub>1</sub> VERSUS R<sub>2</sub> AT TRANSITION POINT

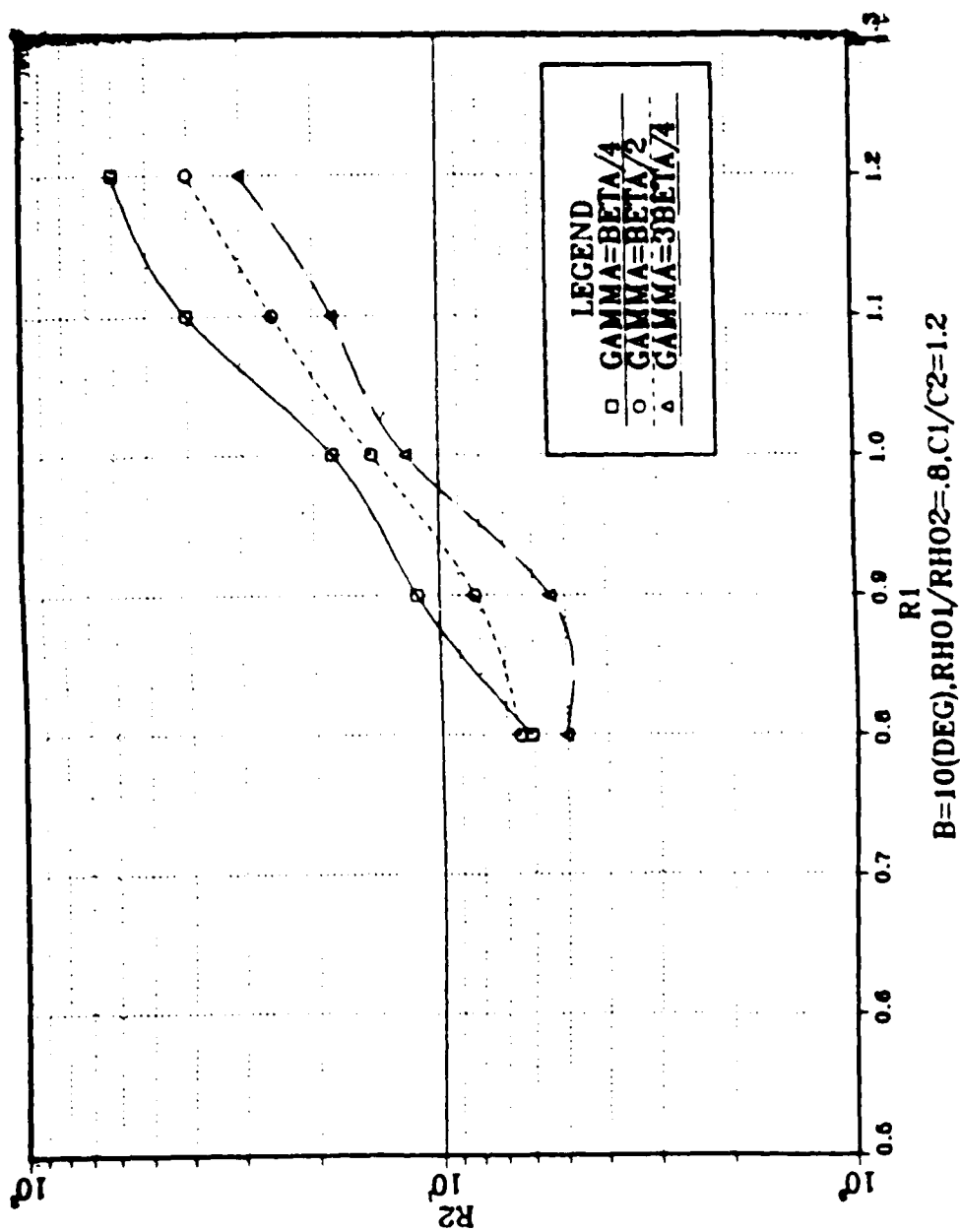


Figure E.8  $R_1$  vs  $R_2$  at the first trans. points, for  $\beta = 10^\circ$ ,  $\rho_1 \rho_2 = 0.90$ ,  $c_1 c_2 = 1.10$ .

## LIST OF REFERENCES

1. C. L. Pekeris, *Theory of Propagation of Explosive Sound in Shallow Water*, Geol. Soc. Am. Mem. 27(1948).
2. L. Brekovskikh, *Waves in Layered Media*, Academic Press, New York, 1960.
3. R. D. Graves, Anton Nagl, H. Uberall and G. L. Zauer, *Range Dependent Normal Modes in Underwater Sound Propagation: Application to the Wedge-Shaped Ocean*, Journal of Acoustical Society of America 58(6), December 1975.
4. J. M. Arnold and L. B. Felsen *Rays and Local Modes in a Wedge-shaped ocean*, Journal of Acoustical Society of America 73(4), April 1983.
5. A. Kamel and L. B. Felsen *Spectral Theory of Sound Propagation in an Ocean Channel with Weakly Sloping Bottom*, Journal of Acoustical Society of America, 73(4), April 1983.
6. Allan D. Pierce, *Guided Mode Disappearance During Upslope Propagation in Variable Depth Shallow Water Overlying a fluid bottom*, Journal of Acoustical Society of America, 72(2), August 1982.
7. Suzanne T. McDaniel, *Parabolic Approximations for Underwater Sound Propagation*, Journal of Acoustical Society of America, 58(6), December 1975.
8. Ding Lee and John S. Papadakis, *Numerical Solutions of the Parabolic Wave Equation: An Ordinary Differential-Equation Approach*,
9. F. B. Jensen and W. A. Kuperman, *Sound Propagation in a Wedge-Shaped Ocean With a Penetrable Bottom*, Journal of Acoustical Society of America, 67(5), May 1980.
10. A. B. Coppens, J. V. Sanders, M. Kawamura, I. Ioannou, *Two Computer Programs for the Evaluation of the Acoustic Pressure Amplitude and Phase of the Bottom of a Wedge-Shaped, Fluid Layer Overlying a Fast Fluid Half-Space*, Naval Postgraduate School, Monterey, CA 93943, December 1978.
11. Chil Ki Baek *The Acoustic Pressure in a Wedge Shaped Water Layer Overlying a Fast Fluid Bottom*, Naval Postgraduate School, M.S. Thesis, March 1984.
12. Patrick S. LeSesne *Development of Computer Programs Using the Method of Images to Predict the Sound Field in a Wedge Overlying a Fast Fluid and Comparison with Laboratory Experiments*, Naval Postgraduate School, M.S. Thesis, December 1984.
13. A. B. Coppens *A Personal Communication* Naval Postgraduate School, Monterey, CA 93943, July 1986.

14. Ioannis Iouannou and Masami Kawamura *Pressure on the Interface between a Converging Fluid Wedge and a Fast Fluid Bottom*, Naval Postgraduate School, M.S. Thesis, December 1978.
15. Kinsler, Frey, Coppens and Sanders, *Fundamentals of Acoustics*, John Wiley & Sons, third edition, 1982

# INITIAL DISTRIBUTION LIST

	No. of Copies
1. Defense Technical Information Center Cameron Station Alexandria, Virginia 22304-6145	2
2. Library, Code 0142 Naval Postgraduate School Monterey, California 93943-5002	2
3. Department Library, Code 61 Department of Physics & Chemistry Naval Postgraduate School Monterey, California 93943-5000	1
4. Dr. A. B. Coppens, Code 61Cz Department of Physics Naval Postgraduate School Monterey, California 93943-5000	2
5. Dr. J. V. Sanders, Code 33A Weapons System Academic Associate Naval Postgraduate School Monterey, California 93943-5000	2
6. CDR Chil Ki Baek SMA 1646, Naval Postgraduate School Monterey, California 93943-5000	1
7. CDR Carolus Kaswandi Dinas Penelitian Dan Pengembangan TNI-AL Jl.Jati, Pangkalan Jati Jakarta Selatan, Indonesia	3
8. Perpustakaan Pusat Markas Besar TNI-AL Cilangkap Jakarta Timur, Indonesia	1
9. Pusat Dokumentasi Ilmiah Nasional JL. Gatot Subroto Jakarta Selatan, Indonesia	2
10. Pusat Pendidikan Ilmu Dan Teknologi TNI-AL Bumi Morokrembangan Surabaya, Indonesia	2

11. Dinas Penelitian Dan Pengembangan TNI-AL 1  
Jl. Jati, Pangkalan Jati  
Jakarta, Indonesia
12. Dr. James Andrews 1  
NSTL Station  
Bay St. Louis, Mississippi 39529
13. Dr. Michael McKissic 1  
Chief of Naval Research  
800 N. Quincy Street  
Arlington, Virginia 22217
14. Mr. Gene Brown 1  
NAVOCEANO, Code 7300  
NSTL Station  
Bay St. Louis, Mississippi 39522
15. Dr. Robert Martin 1  
NORDA 110A  
NSTL Station  
Bay St. Louis, Mississippi 39466
16. Asst. Professor C. Dunlap, Code 68Du 1  
Department of Oceanography  
Naval Postgraduate School  
Monterey, California 93943-5000
17. Marie B. Hashimoto 1  
Department of Aeronautics, Code 67  
Naval Postgraduate School  
Monterey, California 93943-5000



END  
DATE  
FILMED

4-88  
DTIC